



**Kr interference during carbon isotope analysis**

J. Schmitt et al.

Title Page

Abstract

Introduction

Conclusions

References

Tables

Figures



Back

Close

Full Screen / Esc

Printer-friendly Version

Interactive Discussion



# On the interference of $^{86}\text{Kr}^{2+}$ during carbon isotope analysis of atmospheric methane using continuous flow combustion – isotope ratio mass spectrometry

J. Schmitt<sup>1</sup>, B. Seth<sup>1</sup>, M. Bock<sup>1</sup>, C. van der Veen<sup>1</sup>, L. Möller<sup>2</sup>, C. J. Sapart<sup>3</sup>, M. Prokopiou<sup>3</sup>, T. Sowers<sup>3</sup>, T. Röckmann<sup>3</sup>, and H. Fischer<sup>4</sup>

<sup>1</sup>Climate and Environmental Physics, Physics Institute, & Oeschger Centre for Climate Change Research, University of Bern, Sidlerstrasse 5, 3012 Bern, Switzerland

<sup>2</sup>Alfred Wegener Institute for Polar and Marine Research, Bremerhaven, Germany

<sup>3</sup>Institute for Marine and Atmospheric research Utrecht, Utrecht University, Princetonplein 5, 3584CC Utrecht, The Netherlands

<sup>4</sup>Earth and Environment Systems Institute, PennState University, University Park, PA, USA

Received: 12 January 2013 – Accepted: 4 February 2013 – Published: 7 February 2013

Correspondence to: J. Schmitt (schmitt@climate.unibe.ch)

Published by Copernicus Publications on behalf of the European Geosciences Union.

# AMTD

6, 1409–1460, 2013

## Kr interference during carbon isotope analysis

J. Schmitt et al.

Title Page

Abstract

Introduction

Conclusions

References

Tables

Figures



Back

Close

Full Screen / Esc

Printer-friendly Version

Interactive Discussion



## Abstract

Stable carbon isotope analysis of methane ( $\delta^{13}\text{C}$  of  $\text{CH}_4$ ) on atmospheric samples is one key method to constrain the current and past atmospheric  $\text{CH}_4$  budget. A frequently applied measurement technique is gas chromatography isotope ratio mass spectrometry coupled to a combustion-preconcentration unit. This report shows that the atmospheric trace gas krypton can severely interfere during the mass spectrometric measurement leading to significant biases in  $\delta^{13}\text{C}$  of  $\text{CH}_4$  if krypton is not sufficiently separated during the analysis. The effect comes about by the lateral tailing of the peak of doubly charged  $^{86}\text{Kr}$  in the neighbouring  $m/z$ , 44, 45, and 46 Faraday cups. Accordingly, the introduced bias is dependent on the chromatographic separation, the Kr to  $\text{CH}_4$  mixing ratio in the sample, the mass spectrometer source tuning as well as the detector configuration and can amount to up to several permil in  $\delta^{13}\text{C}$ . Apart from technical solutions to avoid this interference we present correction routines to a posteriori remove the bias.

## 1 Introduction

Methane is the third most important greenhouse gas besides water vapour and  $\text{CO}_2$ . The isotopic composition of atmospheric methane ( $\text{CH}_4$ ) provides important constraints on globally integrated  $\text{CH}_4$  sources and sinks. Both the concentration and the isotopic composition of atmospheric  $\text{CH}_4$  in the past have been reconstructed from trapped bubbles in ice cores as well as from the interstitial air in snow pack (firn) on polar glaciers (Miller et al., 2002; Schaefer et al., 2006; Fischer et al., 2008; Kai et al., 2011; Levin et al., 2011; Sowers, 2011; Sapart et al., 2012). Originally, the dual inlet technique coupled to an isotope ratio mass spectrometer (IRMS) was used (Stevens and Rust, 1982; Lowe et al., 1991). With the advent of the continuous flow (CF) technique (Matthews and Hayes, 1978), a growing number of groups have developed systems that allow smaller quantities of  $\text{CH}_4$  to be analyzed, permitting routine analyses on

AMTD

6, 1409–1460, 2013

## Kr interference during carbon isotope analysis

J. Schmitt et al.

Title Page

Abstract

Introduction

Conclusions

References

Tables

Figures

◀

▶

◀

▶

Back

Close

Full Screen / Esc

Printer-friendly Version

Interactive Discussion



**Kr interference during carbon isotope analysis**

J. Schmitt et al.

Title Page

Abstract

Introduction

Conclusions

References

Tables

Figures

◀

▶

◀

▶

Back

Close

Full Screen / Esc

Printer-friendly Version

Interactive Discussion



ice core samples (Merritt et al., 1995; Rice et al., 2001; Miller et al., 2002; Ferretti et al., 2005; Sowers et al., 2005; Schaefer and Whiticar, 2007; Behrens et al., 2008; Umezawa et al., 2009; Melton et al., 2011; Sapart et al., 2011). An overview of these techniques is provided in Table 1. The general procedure for  $\delta^{13}\text{C}\text{-CH}_4$  analysis on air samples using the CF-IRMS technique usually involves several steps to separate a large number of major and trace atmospheric components (see general scheme in Fig. 1). For ice core samples, an additional extraction step either by dry or melt extraction has to be performed first. The purified  $\text{CH}_4$  is then admitted to a combustion interface where  $\text{CH}_4$  is converted to  $\text{CO}_2$ , which is subsequently measured in the IRMS. Here, the most abundant isotopologues of  $\text{CO}_2$  are measured using Faraday cups for the mass to charge ratios ( $m/z$ ) 44, 45 and 46. From these ion beam intensities, the  $\delta^{13}\text{C}$  of  $\text{CH}_4$  is then calculated applying a correction for the isobaric contribution at  $m/z$  45 due to the presence of  $^{12}\text{C}^{17}\text{O}^{16}\text{O}$  (Craig, 1957).

The separation of  $\text{CH}_4$  from the bulk air components ( $\text{N}_2$ ,  $\text{O}_2$  and Ar) and also from minor components like CO is a delicate task. Usually, gas chromatography (GC) is used to separate  $\text{CH}_4$  from CO,  $\text{N}_2$ , and  $\text{CO}_2$ , which would otherwise interfere with the mass spectrometric detection. In this respect, an interference with the atmospheric trace gas krypton has not yet been considered during the method development. The noble gas krypton (Kr) has a natural atmospheric abundance of  $1099 \pm 9$  ppb (Aoki and Makide, 2005) and consists of many stable isotopes, with the most abundant being  $^{84}\text{Kr}$  with 57 % and  $^{86}\text{Kr}$  with 17 %. Although Kr is a trace gas, for several types of samples Kr is as or even more abundant than  $\text{CH}_4$ , e.g. for stratospheric samples (Rice et al., 2003; Röckmann et al., 2011) and air extracted from ice cores. Its atmospheric mixing ratios remained fairly constant over timescales of 100 000 yr with assumed changes being  $< 1$  % between glacial and interglacial climate states due to ocean solubility effects (Headly and Severinghaus, 2007; Ritz et al., 2011).

The physico-chemical properties of  $\text{CH}_4$  and Kr are very similar making them hard to separate one from another. Similar boiling points (Kr = 119 K and  $\text{CH}_4$  = 111 K) make cyro separation impossible and gas chromatographic separation has proven to be very





## 2.2 Bern system

The Bern system is an updated and more versatile follow-up device compared to the AWI system and its description is currently in preparation. While the AWI system is constructed to measure only  $\delta^{13}\text{C}$  of  $\text{CH}_4$ , the Bern system can analyse a larger suite of trace gases ( $\text{CH}_4$ ,  $\text{N}_2\text{O}$  and its stable isotopologues, xenon, ethane, propane, methyl chloride). For that reason the Bern system is equipped with additional technical features allowing special experiments to be performed, e.g. a bypass valve for the combustion oven, and additional valves to inject  $\text{CH}_4$  and Kr mixtures in helium (He) onto the GC system (Fig. 1). Like the AWI system, the Bern system uses a 30-m Carbon-PLOT column, at  $30^\circ\text{C}$  with a flow rate of ca.  $1.0\text{ mL min}^{-1}$ . The Bern system uses the identical Isoprime IRMS equipped with five Faraday cups: The raw data from the mass spectrometer measurements was processed using our in-house isotope software (Bock et al., 2010; Schmitt et al., 2011). After the identification of the Kr interference, two additional traps (pre-combustion trap and post-combustion trap) were installed to get rid of the Kr interference (Sect. 5.3). This new system is referred to as updated Bern system.

## 2.3 IMAU system

A detailed description of the IMAU system is described elsewhere (Brass and Röckmann, 2010; Sapart et al., 2011). A special feature of this system is that it lacks the pre-combustion GC common in other systems (Fig. 1). The IMAU system uses a Thermo Finnigan Delta plus XP as detector. After the Kr interference was identified, the system was modified to remove the interference (Sect. 5.2). As shown in Fig. 1, a GC was added after the conversion of  $\text{CH}_4$  to  $\text{CO}_2$  (post-combustion GC) and this modified system is referred to as updated IMAU system.

## Kr interference during carbon isotope analysis

J. Schmitt et al.

Title Page

Abstract

Introduction

Conclusions

References

Tables

Figures

⏪

⏩

◀

▶

Back

Close

Full Screen / Esc

Printer-friendly Version

Interactive Discussion



## 2.4 PSU system

The measurements done at PSU use the system described earlier in Sowers et al. (2005). The mass spectrometer is a Finnigan MAT 252. Modifications to remove the Kr interference are in process.

## 2.5 Air samples

All four labs measured a set of three cylinders, which were part of an international round robin study. These cylinders were filled at Niwot Ridge, Colorado in 2007 to varying CH<sub>4</sub> concentrations with a balance of ultra high purity air (no CH<sub>4</sub>) to mimic the preindustrial period (~ 900 ppb), the last glacial period (~ 380 ppb) and the present day (1870 ppb). The cylinders were then measured at NOAA to confirm the CH<sub>4</sub> values (GLA, cylinder no. CA01179 = 372 ppb, PI, cylinder no. CC71560 = 904 ppb, and PD, cylinder no. CA03560 = 1831 ppb). While the CH<sub>4</sub> concentration is different, the Kr concentrations of all cylinders should be at natural abundance (1099 ppb), as the GLA and PI cylinders were produced by diluting atmospheric air with CH<sub>4</sub>-free air. The three cylinders have therefore the following CH<sub>4</sub>/Kr mixing ratios [CH<sub>4</sub>/Kr]. 0.33 (GLA), 0.82 (PI) and 1.69 (PD), thus [CH<sub>4</sub>/Kr] covers a range of factor 5. Additionally, cylinder CA08289 (NOAA, Boulder) is used at Bern as a working standard containing 1508.2 ppb CH<sub>4</sub> and IMAU used a natural whole air working standard “GRO” Groningen air with 1967.7 ppb CH<sub>4</sub> for the experiments where pure Kr is added.

## 3 First hints and visual inspection of chromatograms

The possible existence of an interfering compound during the IRMS analysis of  $\delta^{13}\text{C}$  of CH<sub>4</sub> on air samples was first described in 2001 when Rice et al. (2001) described “an unknown contaminant peak”. As the contaminant could not be identified, it remained unclear if this was only a problem of their specific set-up or if it is a general feature of air samples. We believe that this unknown contaminant peak was Kr. In hindsight, it is

### Kr interference during carbon isotope analysis

J. Schmitt et al.

Title Page

Abstract

Introduction

Conclusions

References

Tables

Figures

◀

▶

◀

▶

Back

Close

Full Screen / Esc

Printer-friendly Version

Interactive Discussion





**Kr interference  
during carbon  
isotope analysis**

J. Schmitt et al.

Title Page

Abstract

Introduction

Conclusions

References

Tables

Figures

◀

▶

◀

▶

Back

Close

Full Screen / Esc

Printer-friendly Version

Interactive Discussion



well separated. However, when the two peaks strongly overlap, the influence is less visible. A more sensitive way to identify such interferences in chromatograms is to inspect ion current ratio plots where the background signal has been subtracted from the measured signal to yield the signal of the sample peak only. The plots of this paper show ion current ratios which were corrected for the background signal. Figure 2 shows the three ion current ratios for the time interval around the  $\text{CH}_4$  peak. The retention time of the  $\text{CH}_4$  peak maximum is defined as 0 s. Throughout the paper we label the three ion current ratios according to the involved Faraday cups and the  $m/z$  of the ions which are commonly detected in this cup at  $\text{CO}_2$  tuning: minor1/major (“45/44”), minor2/major (“46/44”), and minor2/minor1 (“46/45”). Note the  $m/z$  pairs are put in parenthesis (e.g. “45/44”) to indicate that only the target ions produced by  $\text{CO}_2$  strictly adhere to this rule. It will be shown in this paper that a small fraction of the  $m/z$  43 beam ( $^{86}\text{Kr}^{2+}$ ) tails all the way into all three cups (major, minor1 and minor2). For the Bern, AWI and IMAU system air samples containing Kr (Fig. 2 black lines) are compared with pure  $\text{CH}_4$  samples (Fig. 2 red lines). For the systems where it was explicitly determined (see below and Figs. 3 and 4), the position of the Kr peak relative to the  $\text{CH}_4$  peak is marked for orientation. As can be seen for all four systems, most ion current ratios of samples containing Kr deviate from the ratios of pure  $\text{CH}_4$ . While these anomalies are well pronounced in all three ratios for the AWI system and resemble a Gaussian shape, the Bern system exhibits no visible anomaly for the “45/44 ratio”, which will be discussed later. In the IMAU case, where Kr was added to a natural air in increasing amounts, one sees that the anomalies become larger with more Kr added. Note that the large anomalies are only the result of large amounts of Kr to an air sample (3-times or 17-times the Kr amount of a natural sample (GRO)). The anomalies of the natural air sample (GRO) are small and hard to detect without prior knowledge. In case of the PSU system, an anomaly is only barely visible for the “45/44 ratio” and obscured by the internal fractionation within the peak (time shift due to mismatch of the resistor capacitor pair). In conclusion, the visual inspection of the ion current ratios of all four systems points to an interfering substance present in natural air samples. The

appearance of this anomaly is specific for each of the four systems and depends on chromatographic separation and properties of the IRMS itself. These anomalies in the ion current ratios can be hidden especially when the background is not subtracted. It requires a careful comparison of the ratios from the natural air sample with those from pure CH<sub>4</sub> to recognise this matrix effect.

## 4 Experiments and results

### 4.1 Simple experiment to identify Kr in the chromatogram

The visual inspection of the chromatograms described above revealed that an interfering compound that we believe is Kr produces anomalies in the ion current ratios. Here we go one step further and provide a test to identify whether the retention time of Kr overlaps with the CH<sub>4</sub> peak. As mentioned above, the behaviour of Kr and CH<sub>4</sub> on GC columns is similar and can result in overlapping peaks with Kr eluting only a few seconds after CH<sub>4</sub>. The following experiment uses the fact that for the electron energies used in the ion source of the IRMS (e.g. 80 eV for the Bern system) ions with two (and sometimes three) electrons removed are also produced (Denifl et al., 2002; King and Price, 2008). Since the optical system of the IRMS separates ions according to their mass to charge ratio ( $m/z$ ), heavy isotopes like <sup>86</sup>Kr can be readily transformed into  $m/z$  43 <sup>86</sup>Kr<sup>2+</sup> ions that strike the imaging plane close to the major ion Faraday cups. Therefore, <sup>86</sup>Kr<sup>2+</sup> ions can be easily monitored by shifting the accelerating voltage (AV) to higher values, e.g. 4030 V instead of 3975 V for the CO<sub>2</sub> focusing for the Bern Isoprime so that the  $m/z$  43 <sup>86</sup>Kr<sup>2+</sup> ions are detected in the normal  $m/z$  44 cup. The  $m/z$  43 beam (<sup>86</sup>Kr<sup>2+</sup>) falls into the major cup, while the  $m/z$  45 beam (mostly <sup>13</sup>C<sup>16</sup>O<sup>16</sup>O) falls into minor2 monitoring the position of the CH<sub>4</sub> peak. This focusing test has the advantage that it can be run on any system with any natural air sample without modifications to the CH<sub>4</sub> separation system. The results of these focusing experiments are shown in Fig. 3. As can be seen in Fig. 3a, the chromatographic separation of

## Kr interference during carbon isotope analysis

J. Schmitt et al.

Title Page

Abstract

Introduction

Conclusions

References

Tables

Figures

⏪

⏩

◀

▶

Back

Close

Full Screen / Esc

Printer-friendly Version

Interactive Discussion



## Kr interference during carbon isotope analysis

J. Schmitt et al.

Title Page

Abstract

Introduction

Conclusions

References

Tables

Figures

◀

▶

◀

▶

Back

Close

Full Screen / Esc

Printer-friendly Version

Interactive Discussion



CH<sub>4</sub> from Kr is about 6 s for the Bern system. Since the peak width (FWHM) for both CH<sub>4</sub> and Kr is also 5–6 s, both peaks do overlap considerably (Fig. 3a) but the overlap is system dependent. From this experiment we can derive the following conclusions. First, a considerable amount of doubly charged Kr ions are produced within the source of the IRMS. Second, <sup>86</sup>Kr<sup>2+</sup> ions allow identifying the retention time of Kr and illustrate that the GC conditions of the Bern and PSU systems are insufficient to separate Kr from CH<sub>4</sub>. Third, the position of the Kr peak and the observed anomalies seen in the ion current ratios (Fig. 2) are similar and suggest that Kr causes these anomalies.

### 4.2 Injections of pure Kr into GC flow

The visual peak inspection and the overlap of CH<sub>4</sub> and Kr from the focusing exercise point to Kr as the source of the interference. However, at this stage it remains unclear how Kr might interfere with the δ<sup>13</sup>C measurement since a direct isobaric effect seems unlikely as none of the Kr isotopes are expected to fall into the given Faraday cups at their nominal *m/z* or *m/2z* (for doubly charged ions) ratios. One possible mechanism generating these anomalies could be that the presence of Kr in the ion source changes the relative ionisation efficiency of the CO<sub>2</sub> isotopologues in the sense of “Ionisation Quench” coined by Meier-Augenstein et al. (2009) In dual inlet applications such matrix interactions of gases in the ion source are commonly termed “chemical slope” (Severinghaus et al., 2003) and refer to differences in the composition of sample and standard gas mixture. While correcting for this effect is common practice, the underlying processes in the ion source are poorly understood.

Alternatively, a more direct effect of Kr could be invoked if deflected Kr ions fell into the Faraday cups. Again, the closest conceivable candidate is the doubly charged Kr isotope <sup>86</sup>Kr<sup>2+</sup> with *m/z* 43. A simple test to distinguish between these two possibilities is the injection of pure Kr. If the pure Kr does not produce a positive signal by itself then the interference relies on the interaction of CO<sub>2</sub> and Kr in the ion source in the sense of a chemical slope. In contrast, if Kr alone generates these signals then some of the

Kr ions are deflected from their expected flight path to fall into Faraday cups with up to 3 units higher  $m/z$  values.

To perform this experiment a mixture of pure Kr in He was injected via the injection loop into the GC flow of the Bern system (see Fig. 1). The amount of injected Kr represents ca. 10 mL STP natural air, thus, a similar amount as is used in our routine ice core measurements. The injected Kr is cryofocused first and then sent to the pre-combustion GC (Fig. 1). After the Kr peak left the GC, the flow passes a dryer before admitting it to the ion source of the IRMS (operated at CO<sub>2</sub> configuration). Note that the combustion oven is bypassed in this experiment to prevent the generation of a small CO<sub>2</sub> peak from trace amounts of residual CH<sub>4</sub> present in the He flow. The results of this experiment are shown in Fig. 4, together with the measurement of a natural air sample. Kr itself produces signals in all Faraday cups at a retention time of ca. 6 s after the usual CH<sub>4</sub> peak maximum (Fig. 4c). This result supports the idea that Kr alone produces the signals detected in the three cups. A comparison with the signal intensities of the air sample (Fig. 4a) shows that the Kr intensities are clearly too small to be directly seen in the air sample itself, e.g. for the minor2 cup the Kr signal is 4 mV at its maximum while for the air sample the minor2 signal is ten times higher. Besides these two basic features, the experiment with pure Kr affords us the opportunity to investigate the general features observed in the ion current ratios of the air sample. A combusted CH<sub>4</sub> sample produces signal intensities (mV) in the three Faraday cups reflecting the natural abundance of the CO<sub>2</sub> isotopologues. For example, the signal of the major cup is a bit higher than the minor 2 signal (Fig. 4a). In contrast, Kr produces a 4-times higher minor2 signal compared to the signal on the major cup (Fig. 4c). In other words, the signals produced by Kr have a very different isotopic fingerprint compared to the CO<sub>2</sub> signals. In this example dealing with minor2 vs major cup (“46/44 ratio”) the Kr signals translate into a very heavy apparent  $\delta^{18}\text{O}$  signature since the  $\delta^{18}\text{O}$  is mainly determined by the “46/44 ratio”. When such an anomaly is added to the signals from combusted CH<sub>4</sub>, the observed “46/44 ratio” will increase as it is the case for the air sample (Fig. 4b, “46/44 ratio”). In contrast, the minor1/major ratio of both the air

## Kr interference during carbon isotope analysis

J. Schmitt et al.

Title Page

Abstract

Introduction

Conclusions

References

Tables

Figures



Back

Close

Full Screen / Esc

Printer-friendly Version

Interactive Discussion



## Kr interference during carbon isotope analysis

J. Schmitt et al.

Title Page

Abstract

Introduction

Conclusions

References

Tables

Figures



Back

Close

Full Screen / Esc

Printer-friendly Version

Interactive Discussion



sample and Kr are comparable, with the signal on minor1 being slightly higher than on major (Fig. 4a and b). Consequently, the signals created by Kr do not produce a visible anomaly in the minor1/major ratio as the “45/44 ratio” of the air sample closely follows the ratio of pure CH<sub>4</sub> (Fig. 4b “45/44 ratio”). Note that this close match of the “45/44” signature of Kr and CO<sub>2</sub> is just a coincidence and only observed for the Bern system. The other three systems show anomalies in the “45/44 ratio” (Fig. 2) which translate into too heavy  $\delta^{13}\text{C}$  values for natural air samples as well. In addition to the more direct influence of the “45/44” anomaly on  $\delta^{13}\text{C}$ , the “46/44” anomaly also alters  $\delta^{13}\text{C}$  of CH<sub>4</sub> samples. This is due to the fact that the <sup>17</sup>O correction algorithm (Craig, 1957; Santrock et al., 1985) relies on assumptions regarding the natural proportions of the stable oxygen isotopes, i.e. the relative contribution of <sup>17</sup>O (<sup>12</sup>C<sup>17</sup>O<sup>16</sup>O with *m/z* 45) and <sup>18</sup>O (<sup>12</sup>C<sup>18</sup>O<sup>16</sup>O with *m/z* 46), which are violated by the Kr signals.

### 4.3 Injection of pure Kr at varied accelerating voltage

The previous experiments clearly showed that Kr is responsible for the observed effects; yet, the underlying mechanism cannot be unambiguously derived from these experiments. From the proximity of the *m/z* 43 beam produced by <sup>86</sup>Kr<sup>2+</sup> we have come up with two hypotheses. The first hypothesis assumes that the observed signals detected in the three Faraday cups are caused by true ions with a mass per charge ratio corresponding to the nominal *m/z* of the cups, i.e. *m/z* 44, *m/z* 45 and *m/z* 46. Since ions with *m/z* 43 are available in the source one might assume that light gases or their ions (e.g. He, H<sub>2</sub> or H) might react with <sup>86</sup>Kr<sup>2+</sup> ions to form molecules or adducts (Leckrone and Hayes, 1998; Sessions et al., 2001) which then could provide the necessary *m/z* 44, *m/z* 45 and *m/z* 46 signals. The other hypothesis assumes that the lateral tail of the *m/z* 43 beam (<sup>86</sup>Kr<sup>2+</sup>) extends all the way to *m/z* 46, thus covering 3 *m/z* units. The fact that the major ion beam contributes some intensity to the neighbouring minor was already observed during the early days of dual inlet-IRMS and termed “pressure effect” or “pressure broadening” and has been treated with abundance sensitivity corrections (Deines, 1970; Mook and Grootes, 1973; Fallick and Baxter, 1977). Peak tailing



## Kr interference during carbon isotope analysis

J. Schmitt et al.

Title Page

Abstract

Introduction

Conclusions

References

Tables

Figures

◀

▶

◀

▶

Back

Close

Full Screen / Esc

Printer-friendly Version

Interactive Discussion



fall into their respective Faraday cups. As a consequence, the  $\delta^{13}\text{C}$  and  $\delta^{18}\text{O}$  values of the rectangular  $\text{CO}_2$  peaks are only slightly affected by these AV shifts (ca. 2% for both  $\delta^{13}\text{C}$  and  $\delta^{18}\text{O}$ , data not shown). In contrast, the maxima of the Kr peaks in the major cup ( $m/z$  44 at PC) increase from ca. 0.5 mV to almost 6 mV, i.e. a factor of 12 as the AV is increased from  $-5\text{V}$  to  $+2\text{V}$  (Fig. 5a). Since the peak heights and areas for minor1 ( $m/z$  45 at PC) and minor2 ( $m/z$  46 at PC) remain fairly constant, the apparent isotopic ratios  $\delta^{13}\text{C}$  and  $\delta^{18}\text{O}$  of the Kr peaks show huge changes reflecting these drastic changes in the beam ratios (Fig. 5b). We calculated these apparent  $\delta^{13}\text{C}$  and  $\delta^{18}\text{O}$  values by integrating the peak areas of the tiny Kr peaks for the three cups and applied the same algorithm as if they were  $\text{CO}_2$  peaks. Our interpretation is that by increasing AV, the amount of  $^{86}\text{Kr}^{2+}$  falling into the major cup quickly increases since the steep tail of this  $m/z$  43 beam is moved closer to the edge of the major cup. The observation of this strong intensity increase on the major cup thus rules out the notion of an ion with  $m/z$  44 producing this interference. However, for the rather constant intensities measured on minor1 and minor2 this experiment cannot rule out the existence of an ion at  $m/z$  45 or  $m/z$  46 since the AV changes were too small to move the centred beam out of the Faraday cup as can be derived from the rather constant  $\delta^{13}\text{C}$  and  $\delta^{18}\text{O}$  values of the  $\text{CO}_2$  rectangular peaks (data not shown) and illustrated in Fig. 7.

Apart from identifying the nature of this interference, this experiment provides valuable information regarding the effects of the Kr interference during sample measurements. From Fig. 5 it is obvious that the apparent  $\delta^{13}\text{C}$  or  $\delta^{18}\text{O}$  signatures of the Kr interference are not constant but depend on the peak centre setting. Consequently, the influence of Kr on the calculated  $\delta^{13}\text{C}$  values of  $\text{CH}_4$  samples is not a constant property for any instrument but both the sign and the magnitude of this effect are sensitive to the setting and stability of the source. As an example, at an AV offset of  $-1.5\text{V}$  with respect to the peak centre the apparent  $\delta^{13}\text{C}$  value of the Kr interference intersects with the range of  $\delta^{13}\text{C}$  values typical for natural  $\text{CH}_4$  samples (around  $-40\%$  to  $-70\%$ , red horizontal line Fig. 5b). If samples are measured at this AV setting, the Kr

## Kr interference during carbon isotope analysis

J. Schmitt et al.

Title Page

Abstract

Introduction

Conclusions

References

Tables

Figures

◀

▶

◀

▶

Back

Close

Full Screen / Esc

Printer-friendly Version

Interactive Discussion



effect on  $\delta^{13}\text{C}$  of  $\text{CH}_4$  will be relatively small and hard to detect. However, for AV offsets  $< -1.5\text{ V}$  the measured  $\delta^{13}\text{C}$  values will be heavier and for AV offsets  $> -1.5\text{ V}$   $\delta^{13}\text{C}$  will become progressively lighter. For  $\delta^{18}\text{O}$ , the Kr bias will always push towards higher values. Note that these values are specific for a certain tuning of a specific instrument.

How subtle differences can produce very different effects can be seen in the results of the AWI and Bern instruments, which have identical IRMS. The AWI system shows a pronounced effect in “45/44” (i.e.  $\delta^{13}\text{C}$ ) while the effect on “45/44” for the Bern instrument is small (compare Fig. 2a and d). Usually, the AV at peak centre is determined automatically during the peak centre procedure, thus the bias could be relatively constant for a certain tuning. However, after performing a peak centre its actual position can move by up to 1 V over the course of hours, thus, generating a time dependent bias on the  $\delta^{13}\text{C}$  values during a measurement, which will add noise to the data set. On the other hand, the close relationship between apparent  $\delta^{13}\text{C}$  and  $\delta^{18}\text{O}$  values provides a means to correct biased  $\delta^{13}\text{C}$  measurements if the expected  $\delta^{18}\text{O}$  value of a sample can be predicted or assumed with good precision. This situation often holds for  $\delta^{13}\text{C}$  since the  $\delta^{18}\text{O}$  value of the  $\text{CH}_4$ -derived  $\text{CO}_2$  is not dependent on the  $\text{CH}_4$  sample but set by the  $\text{O}_2$  used during the combustion process. Therefore, the tight  $\delta^{18}\text{O}$ – $\delta^{13}\text{C}$  correlation seen in Fig. 5b can be used to correct samples which are affected by the Kr interference (see Sect. 5.6).

### 4.3.2 Admission of Kr into the ion source at varied accelerating voltage

The aim of the following experiments is to better characterise the tail of the  $^{86}\text{Kr}^{2+}$  beam using a wider  $m/z$  range. With this experiment we demonstrate that the interferences seen in all three Faraday cups have their origin in the same “master beam”,  $m/z$  43.

To better understand the AV scan with pure Kr, we first present AV scan for  $\text{CO}_2$  (Fig. 6a). For practical reasons, the cups of the triple collector unit (universal collector) of most manufacturers have different widths (resolving slit width) to accommodate multipurpose usage, e.g.  $\delta^{15}\text{N}$  of  $\text{N}_2$ ,  $\delta^{18}\text{O}$  of  $\text{O}_2$ . For the Bern IRMS, an AV change of 85 V

## Kr interference during carbon isotope analysis

J. Schmitt et al.

Title Page

Abstract

Introduction

Conclusions

References

Tables

Figures

◀

▶

◀

▶

Back

Close

Full Screen / Esc

Printer-friendly Version

Interactive Discussion



is roughly equivalent to 1  $m/z$  difference in this mass range. Figure 6b shows the ion current intensities for the three cups in fA for the same AV scan, but with Kr being admitted to the ion source. The  $^{86}\text{Kr}^{2+}$  ion beam with nominally  $m/z$  43.0 starts to fall into the major cup at around +5 V and reaches plateau intensity at +20 V (“transition zone”) with around 600 000 fA (Fig. 6b bottom panel). The blow-up of the major signal reveals that the intensity left from the transition zone (towards higher  $m/z$ ) does not quickly approach zero, but gradually decays when moving to –90 V, i.e. corresponding to ions with a nominal  $m/z$  of already 45 (see Fig. 6a with 85 V corresponding to about 1  $m/z$  unit). The continuation of this tail to even higher  $m/z$  is visible in the signal of minor1, where the intensity decreases from ca. 80 fA at +60 V (corresponding to ca.  $m/z$  44.7) to ca. 30 fA at –90 V (corresponding to ca.  $m/z$  46.0). Similarly, the continuation of the tail is visible in minor2, where the signal becomes almost flat at around 80 fA, covering a range of  $m/z$  45.7 to  $m/z$  47.0. The fact that the Kr tail produces higher intensities for minor2 compared to minor1 reflects the contrasting widths of the two cups: The wider minor2 cup collects ions from a larger mass range of the Kr tail than the smaller minor1 cup (see also scheme of Fig. 7). Again, it is obvious that very small changes in the choice of the peak centre position can have a large effect on the apparent  $\delta^{13}\text{C}$  and  $\delta^{18}\text{O}$  signature of the Kr interference as already seen in Fig. 5b. Further, the flatness of the Kr tail in the region of  $m/z$  45 and  $m/z$  46 explains the strong linear correlation of  $\delta^{13}\text{C}$  and  $\delta^{18}\text{O}$  seen in the other experiments and measured air samples and is the basis for one of the correction methods explained below which rely on a linear relation of the  $m/z$  45 and  $m/z$  46 biases.

#### 4.4 Summary of experiments and concept of Kr interference

Figure 7 shows a schematic drawing which illustrates the involved Faraday cups and the positions of the respective ion beams for  $\text{CO}_2$  and  $^{86}\text{Kr}^{2+}$ . For the construction of the  $^{86}\text{Kr}^{2+}$  tail shown in the lower panels (Fig. 7b and c) we used the data of Figs. 5 and 6. A key characteristic of the Kr interference is that the distribution far outside the

## Kr interference during carbon isotope analysis

J. Schmitt et al.

Title Page

Abstract

Introduction

Conclusions

References

Tables

Figures

◀

▶

◀

▶

Back

Close

Full Screen / Esc

Printer-friendly Version

Interactive Discussion



beam maximum is highly non-Gaussian. Most ions are well focussed into a sharp beam with steep flanks as intensity rapidly drops to  $< 1/1000$  of the plateau level for a 15 V shift in the accelerating voltage (Fig. 6b), corresponding to about 0.2  $m/z$  units. The remarkable feature of the  $^{86}\text{Kr}^{2+}$  beam is that it does not continue this rapid drop but decays only very slowly when its intensity reaches about  $1/10\,000$  of the plateau signal at the 20 V distance from the plateau edge (Fig. 6b). To provide a mathematical model allowing a fat-tailed distribution, a Cauchy distribution was fitted and parameters were selected to resemble the observed data of Figs. 5 and 6b. The positioning of the beams relative to the Faraday cups in the drawing aims to reflect the situation at the peak centre. The plotted distribution (Fig. 7) shows the general features of our experiments with Kr and illustrates the interference, but cannot be used in a quantitative way. Note that the plotted distribution mimicking the lateral tail of the Kr beam represents the signal along the optical plane with the Faraday cups.

While the ion density of the  $^{86}\text{Kr}^{2+}$  beam gradually declines further away from the peak maximum at  $m/z$  43, the transformation from the ion current (apparent fA unit) to the voltage unit (apparent mV unit) overcompensates this drop. As a consequence, the signals (on an apparent mV unit) gained from minor1 and minor2 are higher compared to the major signal. The signal intensities are spatially integrated according to the width of the Faraday cups, the wider the cup the more ions from the tail are collected. The integrated signal from minor2 is higher than the integrated minor1 signal. In summary, the Kr interference signal of a certain Faraday cup is not only a function of the amount of  $m/z$  43, but depends both on the lateral decay of the signal (distribution function towards higher apparent  $m/z$ ) and the width of the Faraday cup.

Using this peak tailing concept, one can explain the following observations:

- pure Kr produces signals at nominal  $m/z$  44 and higher
- the magnitude of the Kr interference depends on the mass spectrometer
- the tuning parameters of the ion source can alter the interferences
- at stable tuning conditions, the effects on  $\delta^{13}\text{C}$  and  $\delta^{18}\text{O}$  are closely correlated

## Kr interference during carbon isotope analysis

J. Schmitt et al.

Title Page

Abstract

Introduction

Conclusions

References

Tables

Figures



Back

Close

Full Screen / Esc

Printer-friendly Version

Interactive Discussion



We want to point out that these observations refer to IRMS measurements in continuous flow mode where He is admitted continuously to the ion source leading to a typical pressure of  $2 \times 10^6$  mbar. In dual inlet mode the source pressure is about factor 10 lower. We have indication from additional tests with dual inlet IRMS measurements (IMAU), where we admitted Kr without He background, that here the Kr interference is less pronounced. Based on these results we speculate that the well focused  $m/z$  43 ion beam is better focussed at dual inlet conditions, but in continuous flow mode it is broadened by collisions with He ions in the source or He atoms in the flight tube. A peak broadening during continuous flow-IRMS compared to dual inlet was also observed during stable sulphur isotope analysis using  $SF_6$  (Ono et al., 2006).

## 5 Solutions for the Kr interference

The observations and experiments discussed above show that Kr can severely interfere with  $\delta^{13}C$  measurements of atmospheric  $CH_4$  samples, if the Kr peak is within the integration boundaries of the  $CH_4$  peak. Given the fact that the Kr interference can produce systematic offsets exceeding the analytical precision, we propose the following strategies to account for this effect.

1. GC separation of Kr from  $CH_4$  prior to conversion to  $CO_2$
2. GC separation of Kr from  $CO_2$  after the  $CH_4$  to  $CO_2$  conversion
3. Cryogenic separation of Kr from  $CO_2$  after the  $CH_4$  to  $CO_2$  conversion
4. Raw data correction using anomalies in the ion current ratios
5. Early peak cut-off at the right integration boundary
6. Correction using relations between  $\delta_{45}$  and  $\delta_{46}$

## Kr interference during carbon isotope analysis

J. Schmitt et al.

Title Page

Abstract

Introduction

Conclusions

References

Tables

Figures

◀

▶

◀

▶

Back

Close

Full Screen / Esc

Printer-friendly Version

Interactive Discussion



It is beyond the scope of this paper to discuss all strategies in great detail. Separate technical papers will deal with the individual solutions applied to a particular system. Instead, we want to provide an overview of possible solutions to let the reader make a first selection on the preferred strategy. The six strategies fall into two classes.

5 Strategies 1 to 3 are technical solutions, which prevent the peak overlap in the ion source, thus avoid the Kr interference for new measurements. Strategies 4 to 6 allow correcting existing datasets. These correction strategies were specifically developed for the existing datasets of the respective systems. As the four systems show different characteristics of the Kr interference, these correction strategies cannot be applied  
10 interchangeably. Consequently, we could not compare the performance of the three correction approaches, but discuss their strengths and limitations individually.

### 5.1 GC separation of Kr from CH<sub>4</sub>

Of all the proposed solutions in this Section, the chromatographic separation of CH<sub>4</sub> from Kr seems to be the most elegant and straightforward way since no additional device is needed besides the basic set up described by Merritt et al. (1995) The only requirement is that the chromatographic separation is good enough to allow a sufficient  
15 separation of CH<sub>4</sub> and Kr. Without knowing that Kr was the “unknown contaminant peak”, Rice et al. (2001) were the first to master this problem with a cryo-GC at  $-50^{\circ}\text{C}$ . To maintain narrow peak width, they used high flow rates of  $2.6\text{ mL min}^{-1}$ , thus a factor 2.5 higher than typically used for ice core analysis. This approach is also applied  
20 by others (Umezawa et al., 2009). Schaefer and Whiticar (2007) followed the same route and used a sub ambient GC at  $0^{\circ}\text{C}$  to separate what they call N<sub>2</sub>O. However, they concluded that separation at  $0^{\circ}\text{C}$  was insufficient and a second GC column was introduced after the combustion oven.

25 With the Bern system, we tested the option to better separate CH<sub>4</sub> from Kr using lower GC temperatures. For the experiments we used a 30-m PoraPLOT column at a flow rate of ca.  $1\text{ mL min}^{-1}$  and measured the chromatographic separation between CH<sub>4</sub> and Kr for three temperatures;  $5^{\circ}\text{C}$ ,  $18^{\circ}\text{C}$ , and  $30^{\circ}\text{C}$ . A Kr-He mixture was injected

## Kr interference during carbon isotope analysis

J. Schmitt et al.

Title Page

Abstract

Introduction

Conclusions

References

Tables

Figures



Back

Close

Full Screen / Esc

Printer-friendly Version

Interactive Discussion



onto the GC flow and cryofocused (Fig. 1). Measurements were done under CO<sub>2</sub> tuning conditions. We did not inject CH<sub>4</sub> but used the small amount of CH<sub>4</sub> cryofocused as blank contribution. This small CH<sub>4</sub> amount turned out to be ideal for these experiments as an amount of CH<sub>4</sub> comparable to samples would otherwise overwhelm the Kr peak.

5 The results are shown in Fig. 8. For 30 °C (Fig. 8a) the separation is only 8 s, thus, insufficient, and results in comparable retention time differences as the CarbonPlot column (ca. 6 s). A reduction to 5 °C (Fig. 8c) shows that the separation of CH<sub>4</sub> from Kr is much better and amounts to 16 s allowing Kr-free δ<sup>13</sup>C analysis of CH<sub>4</sub>. However, this low GC temperate had the disadvantage that N<sub>2</sub>O eluted very late and showed a very broad peak shape, which is not suitable for isotope analysis on N<sub>2</sub>O. Since in our  
10 ice core analysis we measure δ<sup>13</sup>CH<sub>4</sub> and N<sub>2</sub>O isotopes in the same run we did not choose this route but decided to follow the route described in Sect. 5.3.

## 5.2 Chromatographic separation after the CH<sub>4</sub>-CO<sub>2</sub> conversion

The following section describes the separation of Kr from the combusted CH<sub>4</sub> peak using a post-combustion GC column. As shown above and from other studies (Rice et al., 2001), a sufficient separation of CH<sub>4</sub> from Kr requires low GC temperatures due to similar physico-chemical properties of CH<sub>4</sub> and Kr on the GC column. However, after the combustion over the resulting CO<sub>2</sub> is relatively easy to separate from Kr since already at ambient temperatures (e.g. 30 °C) Kr elutes much earlier than CO<sub>2</sub> on  
15 regular GC columns.

The usage of a post-combustion GC column for δ<sup>13</sup>C of CH<sub>4</sub> was first described in Schaefer and Whiticar (2007), who included this device to separate what they interpreted as N<sub>2</sub>O. In the following, we show results from the updated IMAU δ<sup>13</sup>C system, where also a post-conversion GC column is used to tackle the Kr interference (Fig. 1).  
25 The additional component consists of a 12.5 m piece of PoraPlotQ column in a GC which is operated at 24 °C. This GC column was inserted between the Nafion dryer and the open split (see Fig. 1 in Sapart et al., 2011) and provides a separation of Kr

from CO<sub>2</sub> (CH<sub>4</sub>) of about 30 s (Fig. 9b). The figure also nicely shows the response of the IMAU mass spectrometer to pure Kr resulting in a very pronounced peak on the minor2 cup, collecting the nominal  $m/z$  46 ions. A much smaller peak can be seen on minor1 cup (nominal  $m/z$  45). This observation fits to the experiments were pure Kr was added to an air sample and a strong enrichment for  $\delta^{18}\text{O}$  was observed while the enrichment for  $\delta^{13}\text{C}$  was smaller (7.2‰ for  $\delta^{18}\text{O}$ , and 0.79‰ for  $\delta^{13}\text{C}$  for 1 ppm Kr added). In contrast to the Bern system, here the Kr signal on the major cup < 0.1 mV and too small to be visible, thus, the intensities on minor1 and minor2 become fully expressed as anomalies leading to the strong biases in  $\delta^{13}\text{C}$  and  $\delta^{18}\text{O}$  observed for the original IMAU system (compare with the Bern system Figs. 4, 5 and 10).

### 5.3 Cryogenic separation of Kr from CO<sub>2</sub> after the CH<sub>4</sub>-CO<sub>2</sub> conversion

In this section we describe an alternative procedure to separate CO<sub>2</sub> and Kr after the combustion oven, based on the fact that CO<sub>2</sub> can be trapped on a capillary at liquid nitrogen (IN<sub>2</sub>) temperature (-196°C) while Kr passes this trap. In the updated Bern system, such a trap is inserted after the combustion oven (post-combustion trap, Fig. 1). Such a trap not only separates CO<sub>2</sub> from Kr but also acts as a cryofocus yielding narrow, high-intensity CO<sub>2</sub> peaks after the capillary is lifted out of the IN<sub>2</sub> (Melton et al., 2011). A second movable trap is inserted before the combustion oven to trap any residual CO<sub>2</sub> from the GC flow (pre-combustion trap, Fig. 1). With the addition of these two traps, Kr now elutes some 25 s before the sharp CH<sub>4</sub>-derived CO<sub>2</sub> peak, thus, provides baseline separation between the two species (Fig. 10). The timing of the post-combustion trap is a critical parameter of this strategy to avoid trapping traces of combusted sample CO. While most of the CO is removed during the first purification step, a small fraction of CO remains and elutes before the CH<sub>4</sub> peak and becomes combusted to CO<sub>2</sub> as well (Fig. 10b). As can be seen in the example chromatogram, the post combustion trap (trap down arrow in Fig. 10b) is lowered only after the CO-derived CO<sub>2</sub> peak has passed the trap. After a trapping time of 50 s, the capillary is lifted and produces the sharp CO<sub>2</sub> peak. Because Kr is not collected on this capillary its retention

## Kr interference during carbon isotope analysis

J. Schmitt et al.

Title Page

Abstract

Introduction

Conclusions

References

Tables

Figures



Back

Close

Full Screen / Esc

Printer-friendly Version

Interactive Discussion



time is basically the same as without the trap. After the CO<sub>2</sub> peak is measured by the IRMS, a valve is switched to allow the N<sub>2</sub>O peak to bypass the combustion oven (Fig. 1 green circles). Note the different peak shape characteristics of the CH<sub>4</sub>-derived CO<sub>2</sub> peak and the N<sub>2</sub>O peak due to the cryofocusing step.

## 5.4 Subtracting the Kr interference peak from raw data

The above hardware solutions all eliminate the Kr interference. However, extant data sets require an algorithm for correcting for the Kr interference. One method for making the correction relies on the anomalies seen in the ion current ratios, which are particularly pronounced in the data set measured with the AWI system (Fig. 11a). This approach requires the time series of the IRMS acquisition file (raw data file) and software to read and process this data (Bock et al., 2010; Schmitt et al., 2011). With a set of equations the signal intensity of the Kr peak is calculated which produced these anomalies in the first place. The time series of these reconstructed Kr interferences are then subtracted from the measured time series to yield the corrected time series. The latter one is then used to calculate the  $\delta^{13}\text{C}$  values.

In detail, the correction is based on the following equations with  $i$  representing the time series of an ion current and  $R$  the ratio of a pair of ion currents. In case of the AWI measurements the time series covers the interval beginning at the CH<sub>4</sub> peak start and extends to 10 s after the maximum of the CH<sub>4</sub> peak (see Fig. 11b). Note, the following equations and explanation only show the correction of the Kr interference on  $i^{45}$  and  $R^{45/44}$ , the correction for  $i^{46}$  is analogue to the  $i^{45}$  example. We start by assuming the CO<sub>2</sub> peak is pure CO<sub>2</sub> in the ion source, i.e. without Kr interference, the major cup exclusively collects ions with  $m/z$  44 generating the time series of  $i^{44}$ , minor1 only  $m/z$  45 ( $i^{45}$ ), and minor2 only  $m/z$  46 ( $i^{46}$ ). In this case, the ion current ratio  $R_{\text{measured}}^{45/44}$  is the ratio of the two measured ion currents originating exclusively from CO<sub>2</sub> since

## Kr interference during carbon isotope analysis

J. Schmitt et al.

Title Page

Abstract

Introduction

Conclusions

References

Tables

Figures

◀

▶

◀

▶

Back

Close

Full Screen / Esc

Printer-friendly Version

Interactive Discussion



$i_{\text{measured}}^{45}$  equals  $i_{\text{CO}_2}^{45}$  and  $i_{\text{measured}}^{44}$  equals  $i_{\text{CO}_2}^{44}$  given by

$$R_{\text{measured}}^{45/44} = R_{(\text{pure CO}_2)}^{45/44} = i_{\text{CO}_2}^{45}/i_{\text{CO}_2}^{44} = i_{\text{measured}}^{45}/i_{\text{measured}}^{44} \quad (1)$$

However, for a real sample with Kr interference Eq. (1) is not valid for the entire peak. Instead, the entire  $\text{CO}_2$  peak region must be divided into two parts. The left part is dominated by the  $\text{CO}_2$  signals and covers the region from ca. 4 s before the  $\text{CH}_4$  peak maximum to ca. 2 s after the  $\text{CH}_4$  peak maximum (Fig. 11). Equation (1) is only valid for this part. In contrast, the right part is contaminated by Kr. Here, the ion current  $i_{\text{measured}}^{45}$  is the sum of  $i_{\text{CO}_2}^{45}$  and the Kr interference. To generate an anomaly in the ion current ratio of the  $\text{CO}_2$  sample, the ion current ratio of the Kr peak must be different from the ion current ratio of the sample. If the ion current ratios of the interfering signals exactly match those of the sample peak, the  $\delta^{13}\text{C}$  and  $\delta^{18}\text{O}$  values will be unchanged. For that reason, only the  $R^{45/44}$  anomaly to pure  $\text{CO}_2$  is calculated in the following equations, with the part of the total  $i_{\text{Kr}}^{45}$  signal causing this anomaly called  $i_{\text{Kr-excess}}^{45}$ . The sign of  $i_{\text{Kr-excess}}^{45}$  is positive when the minor1/major ratio of the Kr peak is greater than the minor1/major ratio of the pure  $\text{CO}_2$  interval. This case is comparable to the situation of Fig. 4b left side with  $\text{AV} < -2\text{V}$ . Conversely,  $i_{\text{Kr-excess}}^{45}$  can be negative for cases resembling the situation in Fig. 4b right side with  $\text{AV} > -1\text{V}$ . Therefore, for the right side of the peak Eq. (1) is not valid, since  $R_{\text{measured}}^{45/44}$  is the sum of  $i_{\text{CO}_2}^{45}$  and  $i_{\text{Kr-excess}}^{45}$  divided by  $i_{\text{measured}}^{44}$ ,

$$R_{\text{measured}}^{45/44} = R_{(\text{CO}_2+\text{Kr})}^{45/44} = (i_{\text{CO}_2}^{45} + i_{\text{Kr-excess}}^{45})/i_{\text{measured}}^{44} \quad (2)$$

The next step relies on the observation gleaned from the AWI data that all three ion current ratios of pure  $\text{CH}_4$ -derived  $\text{CO}_2$  peaks are essentially flat. In contrast, the ratios of the affected sample peaks show large Kr bumps after the flat plateaus due to Kr signals (Figs. 11a and 2d–f). To calculate a quantitative measure of the Kr interference

## Kr interference during carbon isotope analysis

J. Schmitt et al.

Title Page

Abstract

Introduction

Conclusions

References

Tables

Figures

◀

▶

◀

▶

Back

Close

Full Screen / Esc

Printer-friendly Version

Interactive Discussion



on the ion current ratio, the absolute anomaly of these Kr bumps,  $\Delta R^{45/44}$ , is defined as follows,

$$\Delta R^{45/44} = R_{(\text{CO}_2+\text{Kr})}^{45/44} - R_{(\text{pure CO}_2)}^{45/44} \quad (3)$$

In practice,  $\Delta R^{45/44}$  is calculated by subtracting the “background ratio” defined as  $i^{45}\text{CO}_2/i_{\text{measured}}^{44}$ , from the ratio of the affected right peak side with the contaminated ratio,  $R_{(\text{CO}_2+\text{Kr})}^{45/44}$ . The peak section from which the “background ratio” is calculated is indicated by boxes in Fig. 11a. At this step we make the assumption that without any Kr interference the ratio in the background box would continue all the way to the right side to the right integration boundary (8 to 10 s after  $\text{CH}_4$  peak maximum). This assumption is reasonable at this step for defining the “background ratio” since pure  $\text{CH}_4$  peaks show an almost flat ratio over the whole  $\text{CH}_4$  peak (see Figs. 2d–f and 11a).

Equation (3) can be transformed into Eq. (4), to Eq. (5) and finally into Eq. (6) where the ion current of the excess Kr,  $i_{\text{Kr-excess}}^{45}$ , is isolated.

$$\Delta R^{45/44} = (i_{\text{CO}_2}^{45} + i_{\text{Kr-excess}}^{45})/i_{\text{measured}}^{44} - i_{\text{CO}_2}^{45}/i_{\text{measured}}^{44} \quad (4)$$

$$\Delta R^{45/44} = i_{\text{Kr-excess}}^{45}/i_{\text{measured}}^{44} \quad (5)$$

$$i_{\text{Kr-excess}}^{45} = \Delta R^{45/44} \cdot i_{\text{measured}}^{44} \quad (6)$$

The  $i_{\text{Kr-excess}}^{45}$  time series resembles a Gaussian peak shape with its maximum at the retention time of the Kr peak (Fig. 11b, blue dots), which indicates that the method allows extracting the Kr interference. However, the  $i_{\text{Kr-excess}}^{45}$  is not directly used for the correction but a fit to this time series. This fit is called  $i_{\text{Kr-excess}}^{45 \text{ fitted}}$ . The fit is more accurate and more robust to the selected “background ratio” used in Eq. (3) than the raw

**Kr interference during carbon isotope analysis**

J. Schmitt et al.

Title Page

Abstract

Introduction

Conclusions

References

Tables

Figures



Back

Close

Full Screen / Esc

Printer-friendly Version

Interactive Discussion



$i_{\text{Kr-excess}}^{45}$  time series and the entire Kr peak can be subtracted (see Fig. 11b). Accordingly, the fitting step aims to extract only the part of the  $\Delta R^{45/44}$  anomaly that can be related to a Kr peak (Fig. 11b); for details see the corrected minor1/major ratio (thin line, Fig. 11a) which is not a flat line as it would be the case if the full  $\Delta R^{45/44}$  (raw anomaly) had been removed (Fig. 11a). Using  $i_{\text{Kr-excess fitted}}^{45}$  the measured time series can be corrected as follows

$$i_{\text{corrected}}^{45} = i_{\text{measured}}^{45} - i_{\text{Kr-excess fitted}}^{45} \quad (7)$$

These equations provide a quantitative way to correct for the Kr interference measured on the minor1 cup. To correct the interference on the minor2 cup, equivalent equations for  $i^{46}$  have to be solved. The corrected time series are then fed into by our peak integration software to determine the peak areas within the integration limits of the  $\text{CH}_4$ -derived  $\text{CO}_2$  peak and finally the  $\delta^{13}\text{C}$  value. We have applied this correction to results from the intercalibration cylinders with contrasting  $\text{CH}_4$  mixing ratios ( $\text{CH}_4/\text{Kr}$  ratios) to demonstrate how the interference scales with  $\text{CH}_4$  mixing ratio and to estimate the precision of this correction (Fig. 12a). We see a close linear relationship between the absolute correction,  $\Delta\delta^{13}\text{C}$ , and the inverse  $\text{CH}_4$  mixing ratio ( $1/\text{CH}_4$ ) with  $\Delta\delta^{13}\text{C}$  values of only 0.18‰ for the “present day” cylinder, 0.33‰ for the “pre-industrial” cylinder and 0.81‰ for the “glacial” cylinder of the round robin exercise. The average standard deviation of these values is 0.02‰, thus, the correction algorithm adds only little noise to the results.

In principle, this close linear relationship seen in Fig. 12a can be exploited to correct samples with known  $\text{CH}_4$  mixing ratio in the sense of applying a calibration curve to samples. This approach could be valuable, if samples cannot be corrected individually with the above described algorithm. To evaluate this route, Fig. 12a additionally shows the results from a large data set of ice core samples which were measured with the AWI system. Here we see that the individually corrected samples show a similar  $\text{CH}_4$  dependency as the results from the cylinder measurements, yet the correlation is much

## Kr interference during carbon isotope analysis

J. Schmitt et al.

Title Page

Abstract

Introduction

Conclusions

References

Tables

Figures

⏪

⏩

◀

▶

Back

Close

Full Screen / Esc

Printer-friendly Version

Interactive Discussion



## Kr interference during carbon isotope analysis

J. Schmitt et al.

Title Page

Abstract

Introduction

Conclusions

References

Tables

Figures

◀

▶

◀

▶

Back

Close

Full Screen / Esc

Printer-friendly Version

Interactive Discussion



weaker. The loose connection and the scatter around the regression line of the cylinder results does not reflect the correction method itself, the scatter is rather due to the temporal variability of the Kr effect. While the cylinder measurements were obtained within a few weeks, the ice core data set was measured over a period of two years with some changes in the source focusing parameters. From this we can conclude, that if the  $\Delta\delta^{13}\text{C}$  vs.  $1/\text{CH}_4$  relation is used for correcting affected samples this can be done very precisely when the calibration measurements are done in close proximity to the sample measurements. On the contrary, additional noise is added to the data when measurement and calibration are not performed at the same instrument conditions as the  $\Delta\delta^{13}\text{C}$  vs.  $1/\text{CH}_4$  relation is subject to changes over time.

### 5.5 Early peak cut-off

Another method for correcting extant data for Kr may be employed when there is sufficient separation between the Kr and  $\text{CH}_4$  peaks. The relative position of the Kr and  $\text{CH}_4$  peaks must first be determined as discussed in Sect. 4.1. Once the position of the Kr peak has been established, one can determine when to cut off the  $\text{CH}_4$  peak in order to minimize the Kr interference. There is a trade-off between removing larger portions of the Kr interference that requires larger portions of the sample peak to be removed as well. If we assume that the total Kr effect on  $\delta^{13}\text{C}$  for a sample amounts to 0.8‰, a 90 % cut-off of the Kr peak brings the remaining interference to 0.08‰, i.e. already below the usual measurement precision of ca. 0.1‰ to 0.2‰. With this approach most of the Kr peak is removed, while only about 10 % of the  $\text{CH}_4$  peak is lost. In case of the AWI measurements this translates to a right integration boundary position of 3 s after  $\text{CH}_4$  peak maximum. Clearly, this approach violates the rule that the entire peak must be used for isotope analysis. The consequences can be seen in Fig. 12b. The price for this cut is a higher noise level of ca. 0.35‰ and a systematic bias of ca. 0.2‰ which results from systematic differences of the isotopic ratio along the peak. The results of this simple cutting approach could be improved when a certain peak fraction, i.e. 10 %,

is cut off instead of a fixed time as used here to accommodate for peak shape changes in different chromatograms.

The simplicity of this approach allows for a first check if and to what extent the  $\delta^{13}\text{C}$  data might be influenced by the Kr interference. It also provides confidence in the more sophisticated correction algorithm presented in Sect. 5.4 as it yields a correction of similar magnitude. We applied both the cut-off technique and the subtraction technique on the large ice-core data set measured at AWI and conclude that both correction techniques provide similar  $\delta^{13}\text{C}$ -corrected values (data not shown).

## 5.6 Correction using relations between $\delta 45$ and $\delta 46$

The following section describes a correction routine applied by IMAU. The basis for this correction approach is the fact that the Kr interference affects both the minor1 and the minor2 cup thus  $\delta 45$  ( $\delta^{45/44}$ ) and  $\delta 46$  ( $\delta^{46/44}$ ) as shown in Fig. 13. This leads to biases for both  $\delta^{13}\text{C}$  and  $\delta^{18}\text{O}$ , which show a tight linear relation (e.g. Fig. 5).

A necessary prerequisite to use the  $\delta 45/\delta 46$  relation for correction is the fact that the  $\delta^{18}\text{O}$  of the combustion product  $\text{CO}_2$  is very similar for sample and reference air peaks. This is usually the case because all oxygen atoms of  $\text{CO}_2$  are derived from  $\text{O}_2$  during the combustion process. Consequently, the  $\delta^{18}\text{O}$  deviation of a Kr-affected sample from a pure  $\text{CH}_4$  sample can be ascribed to the influence of the Kr interference on  $\delta^{13}\text{C}$ . Note that this assumption is only valid if sample and the pure  $\text{CH}_4$  are measured closely together, at least at the same day; otherwise the  $\delta^{18}\text{O}$  values are subject to long term drift caused by the redox state of the combustion furnace. To apply this correction, the relation of  $\delta 45/\delta 46$  for the Kr interference has to be acquired. For this, we used the results from the experiments where increasing amounts of Kr were added to a  $\text{CH}_4$  sample (Sect. 3). For the correction, the following equation is used

$$\delta^{13}\text{C}_{\text{corrected}} = \delta^{13}\text{C}_{\text{measured}} - (\delta^{18}\text{O}_{\text{sample}} - \delta^{18}\text{O}_{\text{reference}})\text{slope}_{\delta 45/\delta 46} \quad (8)$$

## Kr interference during carbon isotope analysis

J. Schmitt et al.

Title Page

Abstract

Introduction

Conclusions

References

Tables

Figures

⏪

⏩

◀

▶

Back

Close

Full Screen / Esc

Printer-friendly Version

Interactive Discussion



with  $\delta^{13}\text{C}_{\text{corrected}}$  being the  $\delta^{13}\text{C}$  value after correction,  $\delta^{13}\text{C}_{\text{measured}}$  is the raw measured value,  $\delta^{18}\text{O}_{\text{sample}}$  and  $\delta^{18}\text{O}_{\text{reference}}$  are the  $\delta^{18}\text{O}$  values of the sample and a bracketing reference measurement of pure  $\text{CH}_4$ , and  $\text{slope}_{\delta^{45}/\delta^{46}}$  is the slope of the experiments from Sect. 3 (see Fig. 13).

The value used for the slope is  $\delta^{45}/\delta^{46} = 0.1388\text{‰} \pm 0.0008\text{‰}$ , or approximately 0.14‰ in  $\delta^{13}\text{C}$  for 1‰ in  $\delta^{18}\text{O}$ . Note that for samples the introduced error stemming from the uncertainty of the slope is small and scales with the  $\text{CH}_4/\text{Kr}$  mixing ratio. As an example, for a sample which is corrected by 1.39‰, a typical value for glacial ice samples, the error due to the slope amounts to only 0.008‰, thus, is small compared to the analytical uncertainty of ca. 0.1 to 0.2‰. A second type of error results from the measurement uncertainty of  $\delta^{18}\text{O}$  for both the sample and the reference. Ideally, the measured  $\delta^{18}\text{O}$  values for samples and references should only deviate due to the Kr interference and should be equal for Kr-free  $\text{CH}_4$  samples. However, the  $\delta^{18}\text{O}$  values might vary over time since the conditions of the combustion furnace can change with time. Depending on how and in which intervals the furnace is reoxidised with  $\text{O}_2$ , the variability of  $\delta^{18}\text{O}$  is dependent on the system used and should be checked before this correction technique is used to correct a measured data set of  $\delta^{13}\text{C}$ . Moreover, changes in the IRMS source tuning may change the slope over time. The advantage of this method is that it does not involve special software to do the raw data correction as described in Sect. 6.4. To calibrate this correction, it would suffice to have two gases with known and varying  $\text{CH}_4/\text{Kr}$  ratio.

## 6 Summary and conclusions

This paper identified for the first time that Kr can severely interfere with the measurement of  $\delta^{13}\text{C}$  of  $\text{CH}_4$  during CF-IRMS analysis. The interference for  $\delta^{13}\text{C}$  can be as large as 2‰ if samples are measured which have high Kr to  $\text{CH}_4$  ratios, e.g. air extracted from ice core samples or stratospheric samples, relative to modern atmospheric

### Kr interference during carbon isotope analysis

J. Schmitt et al.

Title Page

Abstract

Introduction

Conclusions

References

Tables

Figures

◀

▶

◀

▶

Back

Close

Full Screen / Esc

Printer-friendly Version

Interactive Discussion



**Kr interference during carbon isotope analysis**

J. Schmitt et al.

Title Page

Abstract

Introduction

Conclusions

References

Tables

Figures

◀

▶

◀

▶

Back

Close

Full Screen / Esc

Printer-friendly Version

Interactive Discussion



air as reference gas. In the ion source of the mass spectrometer the krypton isotope  $^{86}\text{Kr}$  produces doubly charged ions with a  $m/z$  of 43. We demonstrate that the lateral flanks of this ion beam extend several  $m/z$  units and produce an erroneous contribution in all three Faraday cups used for  $\delta^{13}\text{C}$  analysis. The sign and magnitude of this bias is specific for the used instrument and is dependent on the focusing, thus, the bias can change over time. In this sense, the Kr interference can lead to incorrect values, concentration effects (scale effects), drifts over time and simply increase the measurement noise. At constant instrument conditions, the  $\delta^{13}\text{C}$  bias of atmospheric  $\text{CH}_4$  samples inversely scales with the  $\text{CH}_4$  mixing ratio since the Kr mixing ratio can be regarded constant. For example, air samples with lower  $\text{CH}_4$  mixing ratios will yield higher (heavier) apparent  $\delta^{13}\text{C}$  values compared to samples with higher  $\text{CH}_4$  mixing ratios. In the second part of the paper we presented several strategies to tackle the Kr problem. Existing methods can be adapted to either separate Kr from  $\text{CH}_4$  before the combustion process or after conversion to  $\text{CO}_2$ . For existing data sets we propose several correction methods to account for the Kr interference.

Regarding the implications of this effect, we identified the following fields of research using  $\delta^{13}\text{C}$  of  $\text{CH}_4$  where the Kr interference could be relevant if it is not taken into account. The Kr interference is relevant if high accuracy in  $\delta^{13}\text{C}$  is needed and/or samples with low  $\text{CH}_4/\text{Kr}$  ratio mixing ratios are analysed. Note that round robin intercomparison studies aimed to identify offsets between laboratories cannot solve this issue if pure  $\text{CH}_4$  standards, synthetic air mixtures ( $\text{N}_2$ ,  $\text{O}_2$ ) or real samples with only one  $\text{CH}_4/\text{Kr}$  ratio are distributed. Examples for such studies are:

- Palaeo-atmospheric studies on air with low  $\text{CH}_4/\text{Kr}$  mixing ratios (atmospheric  $\text{CH}_4$  mixing ratios as low as 360 ppb), e.g. during the glacial.
- Current atmospheric studies in settings where the atmospheric  $\text{CH}_4/\text{Kr}$  mixing ratio is considerably lowered due to a loss process (e.g. high stratospheric air samples, microbial oxidation in aerobic soils layers).

**Kr interference during carbon isotope analysis**

J. Schmitt et al.

- High precision and accuracy studies of recent atmospheric  $\delta^{13}\text{C}$ . Note that since the late 1990s when many  $\delta^{13}\text{C}$  long term measurements started, by coincidence the atmospheric  $\text{CH}_4$  mixing ratio remained unusually stable.
- Studies analysing the interhemispheric gradient of  $\delta^{13}\text{C}$  which rely on measurements from different measurement systems.
- Fresh or sea water samples which had atmospheric contact having low  $\text{CH}_4/\text{Kr}$  mixing ratios due to higher solubility of Kr compared to  $\text{CH}_4$ .

The compilation shows that the Kr interference is most relevant for the atmospheric community since the demand on accuracy is often high. However,  $\delta^{13}\text{C}$  analyses on  $\text{CH}_4$  in other sample matrixes could be biased by this effect as well. In case of natural water samples, the higher solubility of Kr relative to  $\text{CH}_4$  (about factor 1.8) leads to a lower  $\text{CH}_4/\text{Kr}$  ratio for samples equilibrated with the atmosphere. In settings, where  $\text{CH}_4$  is consumed by methane oxidising bacteria (e.g. deep water samples),  $\text{CH}_4/\text{Kr}$  mixing ratios can approach values as low as  $0.1 \text{ (nmol nmol}^{-1}\text{)}$  (Heeschen et al., 2004). Like for other types of studies where the fractionation factor of a sink process is analysed (e.g. stratospheric samples), any covariation between the  $\text{CH}_4$  concentration and  $\delta^{13}\text{C}$  finally translates in the fractionation factor  $\alpha$ .

The described effect in this paper could also be relevant for other precise measurements using IRMS, where the gas matrix of sample and standard are different and a variable component produces a large beam with a  $m/z$  close to a target mass of the analysed species.

*Acknowledgements.* The work at Bern was supported by the University of Bern, the Swiss National Science Foundation, and the ERC advanced grant project “MATRICs”. The work at Utrecht University was funded by the Dutch Science Foundation (NWO) for funding (Projects: 851.30.020 & 865.07.001). TAS support for this research came from NSF 0944584.

Title Page

Abstract

Introduction

Conclusions

References

Tables

Figures

◀

▶

◀

▶

Back

Close

Full Screen / Esc

Printer-friendly Version

Interactive Discussion



## References

- Aoki, N. and Makide, Y.: The concentration of krypton in the atmosphere – Its revision after half a century, *Chem. Lett.*, 34, 1396–1397, doi:10.1246/cl.2005.1396, 2005.
- Behrens, M., Schmitt, J., Richter, K.-U., Bock, M., Richter, U., Levin, I., and Fischer, H.: A gas chromatography/combustion/isotope ratio mass spectrometry system for high-precision  $\delta^{13}\text{C}$  measurements of atmospheric methane extracted from ice core samples, *Rapid Commun. Mass Spectrom.*, 22, 3261–3269, doi:10.1002/rcm.3720, 2008.
- Bergamaschi, P., Bräunlich, M., Marik, T., and Brenninkmeijer, C. A. M.: Measurements of the carbon and hydrogen isotopes of atmospheric methane at Izana, Tenerife: Seasonal cycles and synoptic-scale variations, *J. Geophys. Res.-Atmos.*, 105, 14531–14546, doi:10.1029/1999JD901176, 2000.
- Bock, M., Schmitt, J., Behrens, M., Möller, L., Schneider, R., Sapart, C., and Fischer, H.: A gas chromatography/pyrolysis/isotope ratio mass spectrometry system for high-precision  $\delta\text{D}$  measurements of atmospheric methane extracted from ice cores, *Rapid Commun. Mass Spectrom.*, 24, 621–633, doi:10.1002/rcm.4429, 2010.
- Bousquet, P., Ciais, P., Miller, J. B., Dlugokencky, E. J., Hauglustaine, D. A., Prigent, C., Van der Werf, G. R., Peylin, P., Brunke, E. G., Carouge, C., Langenfelds, R. L., Lathiere, J., Papa, F., Ramonet, M., Schmidt, M., Steele, L. P., Tyler, S. C., and White, J.: Contribution of anthropogenic and natural sources to atmospheric methane variability, *Nature*, 443, 439–443, doi:10.1038/nature05132, 2006.
- Brass, M. and Röckmann, T.: Continuous-flow isotope ratio mass spectrometry method for carbon and hydrogen isotope measurements on atmospheric methane, *Atmos. Meas. Tech.*, 3, 1707–1721, doi:10.5194/amt-3-1707-2010, 2010.
- Bräunlich, M., Aballanin, O., Marik, T., Jockel, P., Brenninkmeijer, C. A. M., Chappellaz, J., Barnola, J. M., Mulvaney, R., and Sturges, W. T.: Changes in the global atmospheric methane budget over the last decades inferred from  $^{13}\text{C}$  and D isotopic analysis of Antarctic firn air, *J. Geophys. Res.-Atmos.*, 106, 20465–20481, doi:10.1029/2001JD900190, 2001.
- Burford, J. R. and Bremner, J. M.: Gas chromatographic determination of carbon dioxide evolved from soils in closed systems, *Soil Biol. Biochem.*, 4, 191–197, 1972.
- Craig, H.: Isotopic standards for carbon and oxygen and correction factors for mass-spectrometric analysis of carbon dioxide, *Geochim. Cosmochim. Acta*, 12, 133–149, 1957.

AMTD

6, 1409–1460, 2013

### Kr interference during carbon isotope analysis

J. Schmitt et al.

Title Page

Abstract

Introduction

Conclusions

References

Tables

Figures

◀

▶

◀

▶

Back

Close

Full Screen / Esc

Printer-friendly Version

Interactive Discussion



## Kr interference during carbon isotope analysis

J. Schmitt et al.

Title Page

Abstract

Introduction

Conclusions

References

Tables

Figures



Back

Close

Full Screen / Esc

Printer-friendly Version

Interactive Discussion



- Deines, P.: Mass spectrometer correction factors for the determination of small isotopic composition variations of carbon and oxygen, *Int. J. Mass Spectrom. Ion Phys.*, 4, 283–295, 1970.
- Denifl, S., Gstir, B., Hanel, G., Feketeova, L., Matejcek, S., Becker, K., Stamatovic, A., Scheier, P., and Mark, T. D.: Multiple ionization of helium and krypton by electron impact close to threshold: appearance energies and Wannier exponents, *J. Phys. B*, 35, 4685–4694, doi:10.1088/0953-4075/35/22/310, 2002.
- Fallick, A. E. and Baxter, M. S.: Pressure Effect and Peak Broadening in Gas Source Stable Isotope Mass-Spectrometry, *Int. J. Mass Spectrom. Ion Process.*, 25, 155–165, doi:10.1016/0020-7381(77)80046-6, 1977.
- 10 Ferretti, D. F., Miller, J. B., White, J. W. C., Etheridge, D. M., Lassey, K. R., Lowe, D. C., Meure, C. M. M., Dreier, M. F., Trudinger, C. M., van Ommen, T. D., and Langenfelds, R. L.: Unexpected changes to the global methane budget over the past 2000 years, *Science*, 309, 1714–1717, doi:10.1126/science.1115193, 2005.
- 15 Fischer, H., Behrens, M., Bock, M., Richter, U., Schmitt, J., Loulergue, L., Chappellaz, J., Spahni, R., Blunier, T., Leuenberger, M., and Stocker, T. F.: Changing boreal methane sources and constant biomass burning during the last termination, *Nature*, 452, 864–867, doi:10.1038/nature06825, 2008.
- Francey, R. J., Manning, M. R., Allison, C. E., Coram, S. A., Etheridge, D. M., Langenfelds, R. L., Lowe, D. C., and Steele, L. P.: A history of delta  $\delta^{13}\text{C}$  in atmospheric  $\text{CH}_4$  from the Cape Grim Air Archive and Antarctic firn air, *J. Geophys. Res.-Atmos.*, 104, 23631–23643, doi:10.1029/1999JD900357, 1999.
- 20 He, B., Olack, G. A., and Colman, A. S.: Pressure baseline correction and high-precision  $\text{CO}_2$  clumped-isotope ( $\Delta_{47}$ ) measurements in bellows and micro-volume modes, *Rapid Commun. Mass Spectrom.*, 26, 2837–2853, doi:10.1002/rcm.6436, 2012.
- 25 Headly, M. A. and Severinghaus, J. P.: A method to measure  $\text{Kr}/\text{N}_2$  ratios in air bubbles trapped in ice cores and its application in reconstructing past mean ocean temperature, *J. Geophys. Res.-Atmos.*, 112, D19105, doi:10.1029/2006JD008317, 2007.
- Heeschen, K. U., Keir, R. S., Rehder, G., Klatt, O., and Suess, E.: Methane dynamics in the Weddell Sea determined via stable isotope ratios and CFC-11, *Global Biogeochem. Cy.*, 18, GB2012, doi:10.1029/2003GB002151, 2004.
- 30 Kai, F. M., Tyler, S. C., Randerson, J. T., and Blake, D. R.: Reduced methane growth rate explained by decreased Northern Hemisphere microbial sources, *Nature*, 476, 194–197, doi:10.1038/nature10259, 2011.

**Kr interference  
during carbon  
isotope analysis**

J. Schmitt et al.

Title Page

Abstract

Introduction

Conclusions

References

Tables

Figures



Back

Close

Full Screen / Esc

Printer-friendly Version

Interactive Discussion



- Keppler, F., Hamilton, J. T. G., Brass, M., and Röckmann, T.: Methane emissions from terrestrial plants under aerobic conditions, *Nature*, 439, 187–191, doi:10.1038/nature04420, 2006.
- King, S. J. and Price, S. D.: Electron ionization of CO<sub>2</sub>, *Int. J. Mass Spectrom.*, 272, 154–164, doi:10.1016/j.ijms.2008.02.008, 2008.
- 5 Leckrone, K. J. and Hayes, J. M.: Water-Induced Errors in Continuous-Flow Carbon Isotope Ratio Mass Spectrometry, *Anal. Chem.*, 70, 2737–2744, doi:10.1021/ac9803434, 1998.
- Levin, I., Veidt, C., Vaughn, B. H., Brailsford, G., Bromley, T., Heinz, R., Lowe, D., Miller, J. B., Poss, C., and White, J. W. C.: No inter-hemispheric  $\delta^{13}\text{C}\text{H}_4$  trend observed, *Nature*, 486, E3–E4, doi:10.1038/nature11175, 2011.
- 10 Lowe, D. C., Brenninkmeijer, C. A. M., Tyler, S. C., and Dlugkenky, E. J.: Determination of the Isotopic Composition of Atmospheric Methane and its Application in the Antarctic, *J. Geophys. Res.-Atmos.*, 96, 15455–15467, doi:10.1029/91JD01119, 1991.
- Matthews, D. E. and Hayes, J. M.: Isotope-Ratio-Monitoring Gas Chromatography-Mass Spectrometry, *Anal. Chem.*, 50, 1465–1473, doi:10.1021/ac50033a022, 1978.
- 15 Meier-Augenstein, W., Kemp, H. F., and Lock, C. M.: N<sub>2</sub>: a potential pitfall for bulk <sup>2</sup>H isotope analysis of explosives and other nitrogen-rich compounds by continuous-flow isotope-ratio mass spectrometry, *Rapid Commun. Mass Spectrom.*, 23, 2011–2016, doi:10.1002/rcm.4112, 2009.
- Melton, J. R., Whiticar, M. J., and Eby, P.: Stable carbon isotope ratio analyses on trace methane from ice samples, *Chem. Geol.*, 288, 88–96, doi:10.1016/j.chemgeo.2011.03.003, 2011.
- 20 Melton, J. R., Schaefer, H., and Whiticar, M. J.: Enrichment in <sup>13</sup>C of atmospheric CH<sub>4</sub> during the Younger Dryas termination, *Clim. Past*, 8, 1177–1197, doi:10.5194/cp-8-1177-2012, 2012.
- Merritt, D. A., Hayes, J. M., and Des Marais, D. J.: Carbon Isotopic Analysis of Atmospheric Methane by Isotope-Ratio-Monitoring Gas-Chromatography Mass-Spectrometry, *J. Geophys. Res.-Atmos.*, 100, 1317–1326, doi:10.1029/94JD02689, 1995.
- 25 Miller, J. B., Mack, K. A., Dissly, R., White, J. W. C., Dlugokenky, E. J., and Tans, P. P.: Development of analytical methods and measurements of <sup>13</sup>C/<sup>12</sup>C in atmospheric CH<sub>4</sub> from the NOAA Climate Monitoring and Diagnostics Laboratory global air sampling network, *J. Geophys. Res.-Atmos.*, 107, D13, doi:10.1029/2001JD000630, 2002.
- 30 Mischler, J. A., Sowers, T. A., Alley, R. B., Battle, M., McConnell, J. R., Mitchell, L., Popp, T., Sofen, E., and Spencer, M. K.: Carbon and hydrogen isotopic composition of methane

**Kr interference  
during carbon  
isotope analysis**

J. Schmitt et al.

Title Page

Abstract

Introduction

Conclusions

References

Tables

Figures

◀

▶

◀

▶

Back

Close

Full Screen / Esc

Printer-friendly Version

Interactive Discussion



over the last 1000 years, *Global Biogeochem. Cy.*, 23, GB4024, doi:10.1029/2009GB003460, 2009.

Möller, L., Sowers, T., Bock, M., Spahni, R., Behrens, M., Schmitt, J., Miller, H., and Fischer, H.: Strong climate control on emission and isotopic signatures of global methane sources over the last 160,000 years, in preparation, 2013.

Mook, W. G. and Grootes, P. M.: The Measuring Procedure and corrections for the High-Precision mass-spectrometric analysis of isotopic abundance ratios, especially referring to carbon, oxygen and nitrogen, *Int. J. Mass Spectrom. Ion Phys.*, 12, 273–298, 1973.

Ono, S., Wing, B., Rumble, D., and Farquhar, J.: High precision analysis of all four stable isotopes of sulfur ( $^{32}\text{S}$ ,  $^{33}\text{S}$ ,  $^{34}\text{S}$  and  $^{36}\text{S}$ ) at nanomole levels using a laser fluorination isotope-ratio-monitoring gas chromatography-mass spectrometry, *Chem. Geol.*, 225, 30–39, doi:10.1016/j.gca.2006.06.1271, 2006.

Quay, P., Stutsman, J., Wilbur, D., Snover, A., Dlugokencky, E., and Brown, T.: The isotopic composition of atmospheric methane, *Global Biogeochem. Cy.*, 13, 445–461, doi:10.1029/1998GB900006, 1999.

Rice, A. L., Gotoh, A. A., Ajie, H. O., and Tyler, S. C.: High-Precision Continuous-Flow Measurement of  $\delta^{13}\text{C}$  and  $\delta\text{D}$  of Atmospheric  $\text{CH}_4$ , *Anal. Chem.*, 73, 4104–4110, doi:10.1021/ac0155106, 2001.

Rice, A. L., Tyler, S. C., McCarthy, M. C., Boering, K. A., and Atlas, E.: Carbon and hydrogen isotopic compositions of stratospheric methane: 1. High-precision observations from the NASA ER-2 aircraft, *J. Geophys. Res.-Atmos.*, 108, D15, doi:10.1029/2002JD003042, 2003.

Ritz, S. P., Stocker, T. F., and Severinghaus, J. P.: Noble gases as proxies of mean ocean temperature: sensitivity studies using a climate model of reduced complexity, *Quaternary Sci. Rev.*, 30, 3728–3741, doi:10.1016/j.quascirev.2011.09.021, 2011.

Röckmann, T., Brass, M., Borchers, R., and Engel, A.: The isotopic composition of methane in the stratosphere: high-altitude balloon sample measurements, *Atmos. Chem. Phys.*, 11, 13287–13304, doi:10.5194/acp-11-13287-2011, 2011.

Santrock, J., Studley, S. A., and Hayes, J. M.: Isotopic analyses based on the mass spectrum of carbon dioxide, *Anal. Chem.*, 57, 1444–1448, 1985.

Sapart, C. J., van der Veen, C., Vigano, I., Brass, M., van de Wal, R. S. W., Bock, M., Fischer, H., Sowers, T., Buizert, C., Sperlich, P., Blunier, T., Behrens, M., Schmitt, J., Seth, B., and Röckmann, T.: Simultaneous stable isotope analysis of methane and nitrous oxide on ice core samples, *Atmos. Meas. Tech.*, 4, 2607–2618, doi:10.5194/amt-4-2607-2011, 2011.

**Kr interference  
during carbon  
isotope analysis**

J. Schmitt et al.

Title Page

Abstract

Introduction

Conclusions

References

Tables

Figures



Back

Close

Full Screen / Esc

Printer-friendly Version

Interactive Discussion



- Sapart, C. J., Monteil, G., Prokopiou, M., van de Wal, R. S. W., Kaplan, J. O., Sperlich, P., Krumhardt, K. M., van der Veen, C., Houweling, S., Krol, M. C., Blunier, T., Sowers, T., Martinerie, P., Witrant, E., Dahl-Jensen, D., and Röckmann, T.: Natural and anthropogenic variations in methane sources during the past two millennia, *Nature*, 490, 85–88, doi:10.1038/nature11461, 2012.
- Schaefer, H., Whiticar, M. J., Brook, E. J., Petrenko, V. V., Ferretti, D. F., and Severinghaus, J. P.: Ice record of  $\delta^{13}\text{C}$  for atmospheric  $\text{CH}_4$  across the Younger Dryas-Preboreal transition, *Science*, 313, 1109–1112, doi:10.1126/science.1126562, 2006.
- Schaefer, H. and Whiticar, M. J.: Measurement of stable carbon isotope ratios of methane in ice samples, *Organ. Geochem.*, 38, 216–226, doi:10.1016/j.orggeochem.2006.10.006, 2007.
- Schmitt, J., Schneider, R., and Fischer, H.: A sublimation technique for high-precision measurements of  $\delta^{13}\text{CO}_2$  and mixing ratios of  $\text{CO}_2$  and  $\text{N}_2\text{O}$  from air trapped in ice cores, *Atmos. Meas. Tech.*, 4, 1445–1461, doi:10.5194/amt-4-1445-2011, 2011.
- Schüpbach, S., Federer, U., Kaufmann, P. R., Hutterli, M. A., Buiron, D., Blunier, T., Fischer, H., and Stocker, T. F.: A New Method for High-Resolution Methane Measurements on Polar Ice Cores Using Continuous Flow Analysis, *Environ. Sci. Technol.*, 43, 5371–5376, doi:10.1021/es9003137, 2009.
- Sessions, A. L., Burgoyne, T. W., and Hayes, J. M.: Correction of  $\text{H}^{3+}$  contributions in hydrogen isotope ratio monitoring mass spectrometry, *Anal. Chem.*, 73, 192–199, doi:10.1088/0953-4075/35/22/310, 2001.
- Severinghaus, J. P., Grachev, A., Luz, B., and Caillon, N.: A method for precise measurement of argon 40/36 and krypton/argon ratios in trapped air in polar ice with applications to past firn thickness and abrupt climate change in Greenland and at Siple Dome, Antarctica, *Geochim. Cosmochim. Acta*, 67, 325, doi:10.1016/S0016-7037(02)00965-1, 2003.
- Sowers, T., Bernard, S., Aballain, O., Chappellaz, J., Barnola, J. M., and Marik, T.: Records of the  $\delta^{13}\text{C}$  of atmospheric  $\text{CH}_4$  over the last 2 centuries as recorded in Antarctic snow and ice, *Global Biogeochem. Cy.*, 19, 1, doi:10.1029/2004GB002408, 2005.
- Sowers, T.: Atmospheric methane isotope records covering the Holocene period, *Quaternary Sci. Rev.*, 29, 213–221, doi:10.1016/j.quascirev.2009.05.023, 2011.
- Stevens, C. M. and Rust, F. E.: The Carbon Isotopic Composition of Atmospheric Methane, *J. Geophys. Res.-Ocean. Atmos.*, 87, 4879–4882, doi:10.1029/JC087iC07p04879, 1982.
- Tyler, S. C., Ajie, H. O., Gupta, M. L., Cicerone, R. J., Blake, D. R., and Dlugokencky, E. J.: Stable carbon isotopic composition of atmospheric methane: A comparison of surface level and free

tropospheric air, J. Geophys. Res.-Atmos., 104, 13895–13910, doi:10.1029/1999JD900029, 1999.

5 Tyler, S. C., Rice, A. L., and Ajie, H. O.: Stable isotope ratios in atmospheric CH<sub>4</sub>: Implications for seasonal sources and sinks, J. Geophys. Res.-Atmos., 112, D03303, doi:10.1029/2006JD007231, 2007.

Umezawa, T., Aoki, S., Nakazawa, T., and Morimoto, S.: A High-precision Measurement System for Carbon and Hydrogen Isotopic Ratios of Atmospheric Methane and Its Application to Air Samples Collected in the Western Pacific Region, J. Meteorol. Soc. Jpn, 87, 365–379, doi:10.2151/jmsj.87.365, 2009.

10 Vigano, I., Röckmann, T., Holzinger, R., van Dijk, A., Keppler, F., Greule, M., Brand, W. A., Geilmann, H., and van Weelden, H.: The stable isotope signature of methane emitted from plant material under UV irradiation, Atmos. Environ., 43, 5637–5646, doi:10.1016/j.atmosenv.2009.07.046, 2009.

AMTD

6, 1409–1460, 2013

## Kr interference during carbon isotope analysis

J. Schmitt et al.

Title Page

Abstract

Introduction

Conclusions

References

Tables

Figures

◀

▶

◀

▶

Back

Close

Full Screen / Esc

Printer-friendly Version

Interactive Discussion



## Kr interference during carbon isotope analysis

J. Schmitt et al.

Title Page

Abstract

Introduction

Conclusions

References

Tables

Figures

◀

▶

◀

▶

Back

Close

Full Screen / Esc

Printer-friendly Version

Interactive Discussion



**Table 1.** Collection of publications dealing with  $\delta^{13}\text{C}\text{-CH}_4$  measurements in view of possible Kr interferences. The collection is not exhaustive and lists only some of the publications in the field of ice core and atmospheric measurements. To allow a faster orientation, which data set is produced by which method, we used the following scheme: technical paper (data paper).

Publication	Pre-combustion GC	Technical details and remarks
<i>dual inlet techniques:</i>		
Stevens and Rust (1982) (Quay et al., 1999), Lowe et al. (1991) (Francey et al., 1999), Tyler et al. (1999) (Tyler et al., 2007) Bergamaschi et al. (2000)	No GC, only CO is removed prior to combustion. Ethane and other NMHC are combusted as well but due to low conc. compared to CH <sub>4</sub> the effect is small.	Prior to the conversion of CH <sub>4</sub> to CO <sub>2</sub> , atmospheric CO <sub>2</sub> is removed from the air stream. After the combustion unit, the produced CO <sub>2</sub> is trapped at IN <sub>2</sub> , thus, separating it from Kr.
<i>continuous flow techniques:</i>		
Merritt et al. (1995)	PoraPLOT Q, 25 m, 0.32 mm i.d., 20–25 °C, 1 mL min <sup>-1</sup>	no special measures to separate Kr from CH <sub>4</sub>
Rice et al. (2001) (Rice et al., 2003)	PoraPLOT Q, 25 m, 0.32 mm i.d., GC temperature ramped from –50 °C to 30 °C, 2.6 mL min <sup>-1</sup>	GC with cryogenic unit to allow separation of CH <sub>4</sub> from an “unknown contaminant peak that otherwise interferes with masses 45 and 46”
Bräunlich et al. (2001)	MPI: = Bergamaschi et al. (2000); LGGE: GS-Q, 30 m, 0.32 mm i.d.	For the MPI data set Kr is separated from CO <sub>2</sub> (CH <sub>4</sub> ). For LGGE, Kr might coelute with CH <sub>4</sub> .
Behrens et al. (2008) (Fischer et al., 2008)	CarbonPLOT, 30 m, 0.32 mm i.d., 30 °C, 1.1 mL min <sup>-1</sup>	no special measures to separate Kr from CH <sub>4</sub>
Miller et al. (2002) (Ferretti et al., 2005; Bousquet et al., 2006)	Molecular Sieve 5A, 80 °C, 2.0 mL min <sup>-1</sup>	Separation of CH <sub>4</sub> and Kr on this column is unknown
Sowers et al. (2005) (Mischler et al., 2009)	PoraPLOT Q, 30 m, 0.32 mm i.d.	no special measures to separate Kr from CH <sub>4</sub>
Schaefer and Whiticar (2007) (Schaefer et al., 2006)	GSQ PLOT, 30 m, 0.53 mm i.d., 0 °C, 1 mL min <sup>-1</sup>	Kr is separated from CO <sub>2</sub> by the post combustion GC
Umezawa et al. (2009)	PoraPLOT Q, 25 m, 0.32 mm i.d., –30 °C, 3.0 mL min <sup>-1</sup>	GC with cryogenic unit to separate CH <sub>4</sub> from an unknown contaminant peak
Melton et al. (2011) (Melton et al., 2012)	GSQ PLOT, 30 m, 0.53 mm i.d., 25 °C, 1 mL min <sup>-1</sup>	post combustion trap followed by an additional GC (GSQ PoraPLOT, 30 m, 0.53 mm i.d., 25 °C) separates Kr from CH <sub>4</sub> -derived CO <sub>2</sub> .
Brass and Röckmann (2010); Sapart et al. (2011) (Keppler et al., 2006; Vígano et al., 2009; Röckmann et al., 2011; Sapart et al., 2012)	No pre combustion GC	Purification relies on Precon and Cryofocus, as a replacement of the omitted pre combustion GC

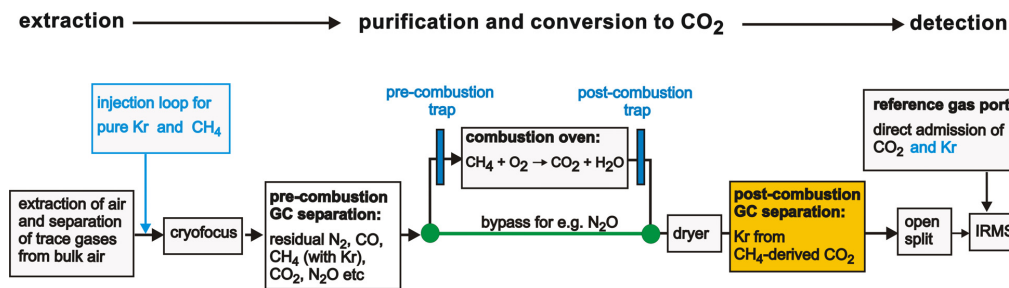


**Fig. 1.** Simplified flow scheme used for  $\delta^{13}\text{C}$  analysis of  $\text{CH}_4$  on air samples applying the continuous flow-IRMS technique. The scheme provides an overview of basic components and specific add-ons of the systems used in this study. The analysis comprises three main steps (from left to right: extraction, purification and combustion of  $\text{CH}_4$  to  $\text{CO}_2$ , and finally the detection in the isotope ratio mass spectrometer). The grey boxes represent the basic components used by all laboratories and date back to the milestone publications in this field (Merritt et al., 1995; Rice et al., 2001). An exception is the IMAU system described by Sapart et al. (2011), where no pre-combustion GC is used and the separation of the gases is achieved solely by a preconcentration step. Coloured symbols denote additional devices, which are specific for the certain laboratory. Blue and green colours denote features of the Bern system, while the yellow box is specific for the updated IMAU system. The injection loop (blue box) allows injecting pure  $\text{CH}_4$  and Kr into the GC flow to monitor the system and allow special experiments. The pre-combustion trap and the post-combustion trap were included later on into the updated Bern system to remove the Kr interference. The yellow box represents the post-combustion GC which was included in the updated IMAU system to remove the Kr interference.

## Kr interference during carbon isotope analysis

J. Schmitt et al.

Title Page

Abstract

Introduction

Conclusions

References

Tables

Figures

◀

▶

◀

▶

Back

Close

Full Screen / Esc

Printer-friendly Version

Interactive Discussion



## Kr interference during carbon isotope analysis

J. Schmitt et al.

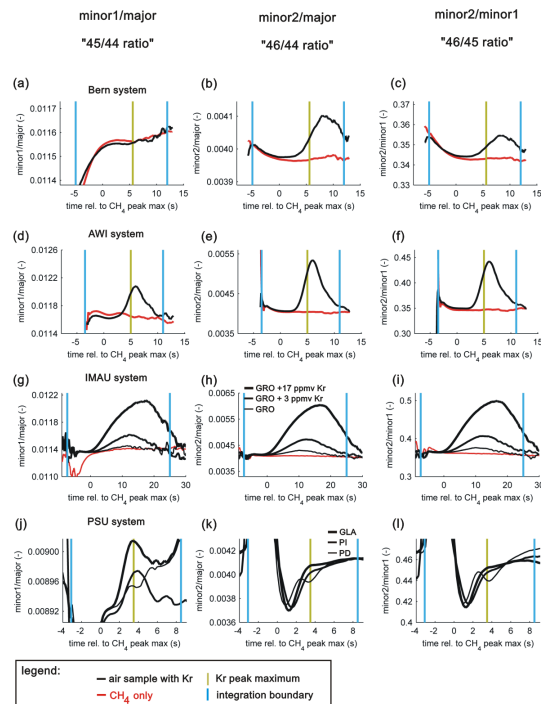


**Fig. 2.** Comparison of the ion current ratios of the four systems (from top to bottom: Bern, AWI, IMAU, PSU). The left column shows the minor1/major ratio (“45/44 ratio”); the middle column shows minor2/major (“46/44 ratio”), the right column minor2/minor1 (“46/45 ratio”). Natural air samples and air samples with added Kr are plotted as black lines and injections of pure  $\text{CH}_4$  are shown as red lines illustrating the anomalies seen in the Kr containing samples. Blue vertical lines mark the left and right integration limits. Green vertical lines mark the maximum position of the Kr peak where we could determine its precise position. The Kr interference in the AWI system is visually more pronounced compared to the Bern system due to the differences in peak separation and focusing of the IRMS.

## Kr interference during carbon isotope analysis

J. Schmitt et al.

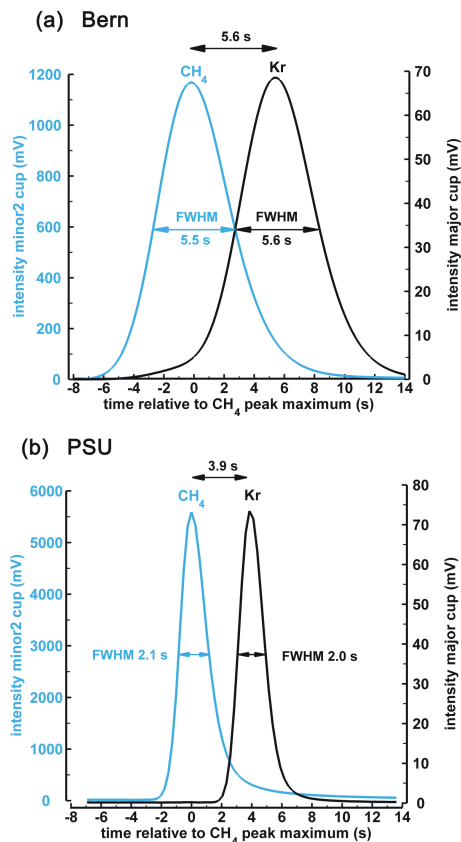


**Fig. 3.** Chromatogram of an atmospheric air sample showing the separation of  $\text{CH}_4$  from Kr for the Bern-system (a) and the PSU system (b). The ion source of the IRMS were focused thus that the  $m/z$  43 beam of  $^{86}\text{Kr}^{2+}$  falls into the major cup (black line, right axis). The isotopologues of  $\text{CO}_2$  with  $m/z$  45 fall into the minor2 cup and mark the position of the  $\text{CH}_4$  peak (blue line, left axis).

Title Page

Abstract

Introduction

Conclusions

References

Tables

Figures

◀

▶

◀

▶

Back

Close

Full Screen / Esc

Printer-friendly Version

Interactive Discussion



## Kr interference during carbon isotope analysis

J. Schmitt et al.

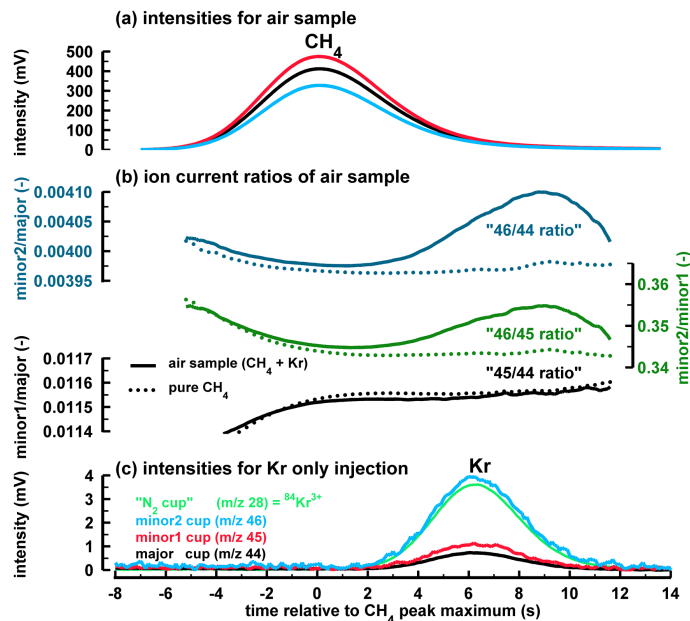


**Fig. 4.** Comparison of a CH<sub>4</sub> peak of an air sample with the signals gained from an injection of pure Kr measured with the Bern system at CO<sub>2</sub> tuning conditions **(a)** Beam intensities in mV for the CH<sub>4</sub> sample peak (369 ppb CH<sub>4</sub> with natural abundance of Kr) with the retention time centred to the CH<sub>4</sub> peak maximum. **(b)** Background corrected ion current ratios, “46/44 ratio” in blue, “46/45 ratio” in green and “45/44 ratio” in black of the atmospheric air sample (solid line) and pure CH<sub>4</sub> (dotted line) illustrating the anomalies seen in “46/44” and “46/45” but no visible effect on “45/44”. Panel **(c)** shows the beam intensities for a measurement where Kr was injected into the GC flow. Due to the chromatographic effect of the GC column, the retention time of the Kr peak is ca. 6 s longer than the CH<sub>4</sub> peak, yet there is a considerable overlap. Note the signal measured at  $m/z$  28 (“N<sub>2</sub> cup”) can be directly related to <sup>84</sup>Kr<sup>3+</sup> which has the exact  $m/z = 28$  value.

## Kr interference during carbon isotope analysis

J. Schmitt et al.

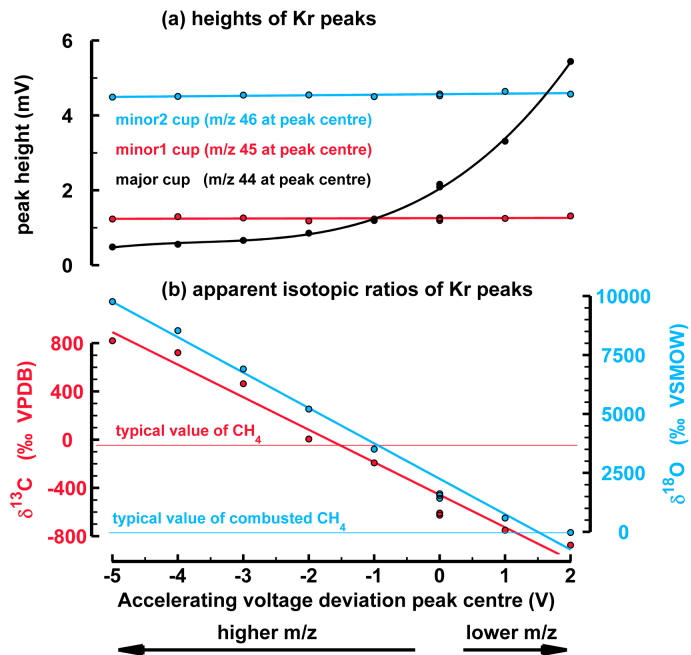


**Fig. 5.** Influence of slight changes in the accelerating voltage on the peak heights and apparent isotopic signatures of Kr peaks. Results of Kr injection into GC flow carried out with the Bern system with the source tuned to  $\text{CO}_2$ . **(a)** The upper panel shows the measured peak heights for the three Faraday cups (major, minor1, minor2) of the Kr peak as a function of the accelerating voltage; dots represent measurements and lines a linear fit for minor1 and minor2, and a cubic fit for the major cup. **(b)** The lower panel shows the apparent isotopic composition ( $\delta^{13}\text{C}$  in red and  $\delta^{18}\text{O}$  in blue) of the Kr interference calculated from the peak area of the Kr peaks; dots represent measurements and lines the linear fits.

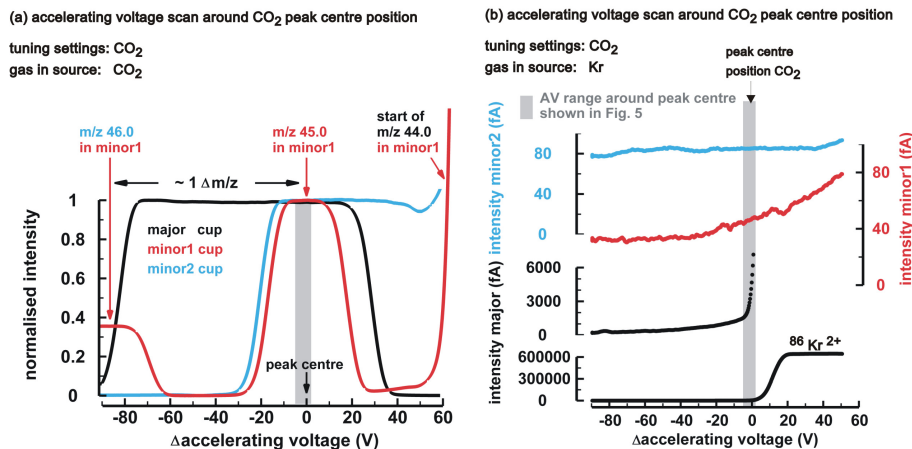


**Fig. 6.** Accelerating voltage (AV) scans around the peak centre position of CO<sub>2</sub> measured with the Bern system. The plots show beam intensities as a function of  $\Delta AV$ , i.e. the differences to the AV at peak centre position at 3975 V. **(a)** AV scan with CO<sub>2</sub> from the reference port with normalised beam intensities for the three Faraday cups. The different peak widths reflect the geometric widths of the cups from small (minor1) to intermediate (minor2) to wide (major). **(b)** AV scan with Kr admitted by an additional valve at the Isoprime ref gas box showing the evolution of the Kr interference over a wide  $m/z$  range covering all three Faraday cups. The intensities are plotted in fA, thus, proportional to the number of ions collected in the cup. For the major cup, the full range is shown in the bottom panel covering the plateau (600 000 fA at  $\Delta AV > 20$  V). The zoomed version of the major cup allows a better inspection of this signal decay to values  $< 1000$  fA. The intensity of the  $^{86}\text{Kr}^{2+}$  beam progressively decays in the  $m/z$  45 region, as monitored by the minor1 cup and becomes almost flat at around  $m/z$  46 (minor2 cup). Note the intensities measured with the minor2 cup are ca. factor 2 higher than for minor1 mirroring the different widths of the two cups.

## Kr interference during carbon isotope analysis

J. Schmitt et al.

Title Page

Abstract

Introduction

Conclusions

References

Tables

Figures

◀

▶

◀

▶

Back

Close

Full Screen / Esc

Printer-friendly Version

Interactive Discussion



## Kr interference during carbon isotope analysis

J. Schmitt et al.

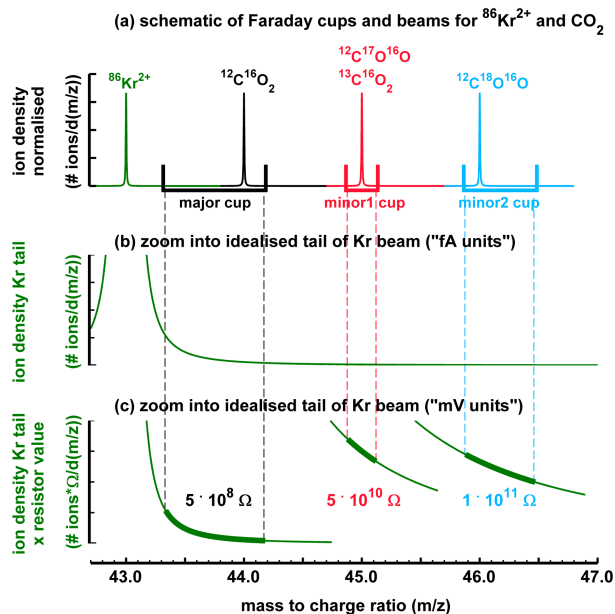


**Fig. 7.** Schematic showing the Faraday cups and the involved ion beams of  $\text{CO}_2$  and  $^{86}\text{Kr}^{2+}$  to help visualise the observed Kr interference during  $\delta^{13}\text{C}$  analysis as observed with the Bern IRMS (a) Estimated positioning and width of the Faraday cups and the position of the respective ion beams ( $m/z$ ) of the  $\text{CO}_2$  isotopologues and  $^{86}\text{Kr}^{2+}$ . (b) To illustrate the broad tailing of the  $m/z$  43 beam ( $^{86}\text{Kr}^{2+}$ ) into the region of higher  $m/z$ , an artificial density distribution (Cauchy) is used to provide a reasonable lateral distribution of the produced  $^{86}\text{Kr}^{2+}$  ions. For (c) the same ion density distribution is used as in (b), but ion densities were converted to a mV unit using the respective values of the feedback resistors of the Bern Isoprime machine; the thick line represents that part of the continuous beam which becomes finally collected in the respective Faraday cups (vertical dashed lines mark the geometric limits of the Faraday cups) as a visualisation of the spatial integration of the Faraday cup).

## Kr interference during carbon isotope analysis

J. Schmitt et al.

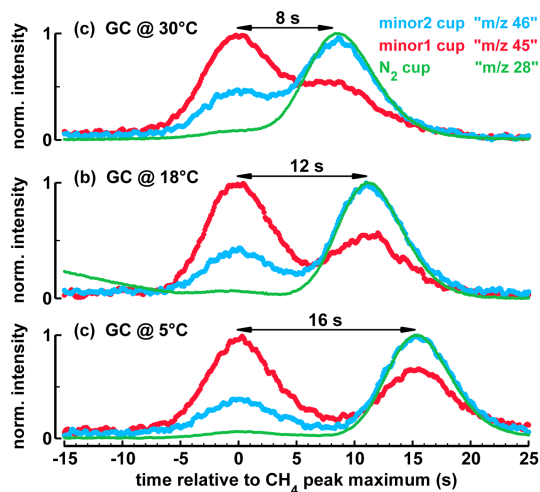


**Fig. 8.** Chromatograms showing the separation between  $\text{CH}_4$  (left peak) and Kr (right peak) on a PoraPLOT column for 30°C, 18°C and 5°C measured with the Bern system. The Kr interference is visible in all Faraday cups, either as a direct signal of  $^{84}\text{Kr}^{3+}$  in the  $m/z$  28 cup (thin green line), or from the  $^{86}\text{Kr}^{2+}$  tail for the minor1 and minor 2 (thick red and blue, respectively).

Title Page

Abstract

Introduction

Conclusions

References

Tables

Figures

◀

▶

◀

▶

Back

Close

Full Screen / Esc

Printer-friendly Version

Interactive Discussion



## Kr interference during carbon isotope analysis

J. Schmitt et al.

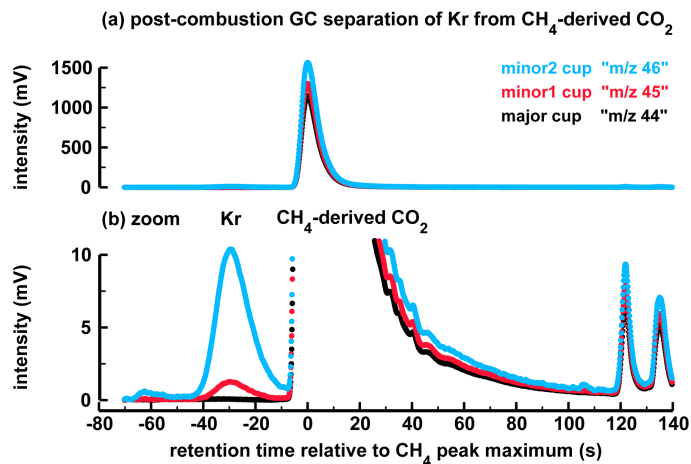


**Fig. 9.** Chromatogram showing the separation of Kr from  $\text{CO}_2$  achieved with the improved IMAU system, which includes a GC column after the combustion oven. Due to the additional GC, Kr elutes before instead of after the  $\text{CH}_4$ -derived  $\text{CO}_2$  peak as shown in the chromatograms of Fig. 3.

[Title Page](#)[Abstract](#)[Introduction](#)[Conclusions](#)[References](#)[Tables](#)[Figures](#)[⏪](#)[⏩](#)[◀](#)[▶](#)[Back](#)[Close](#)[Full Screen / Esc](#)[Printer-friendly Version](#)[Interactive Discussion](#)

## Kr interference during carbon isotope analysis

J. Schmitt et al.

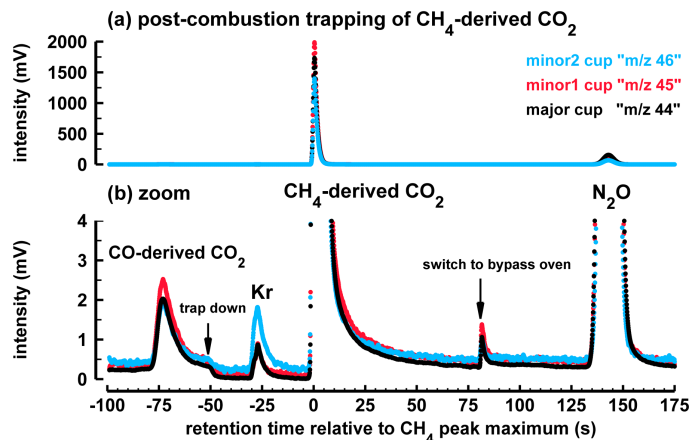


**Fig. 10.** Sample chromatogram showing the separation of Kr from CH<sub>4</sub>-derived CO<sub>2</sub> for the improved Bern system. **(a)** Full range plot of the narrow, cryofocused CH<sub>4</sub>-derived CO<sub>2</sub> peak and the broader N<sub>2</sub>O peak without cryofocusing step. **(b)** Zoomed plot to see the separation of Kr from CH<sub>4</sub>-derived CO<sub>2</sub>. The arrow “trap down” marks the time when the capillary is lowered into IN<sub>2</sub> to trap the CO<sub>2</sub> from the combustion oven. While CO<sub>2</sub> becomes trapped at IN<sub>2</sub> temperature, Kr passes the capillary without delay and shows the typical Kr interference signal.

[Title Page](#)[Abstract](#)[Introduction](#)[Conclusions](#)[References](#)[Tables](#)[Figures](#)[◀](#)[▶](#)[◀](#)[▶](#)[Back](#)[Close](#)[Full Screen / Esc](#)[Printer-friendly Version](#)[Interactive Discussion](#)

## Kr interference during carbon isotope analysis

J. Schmitt et al.

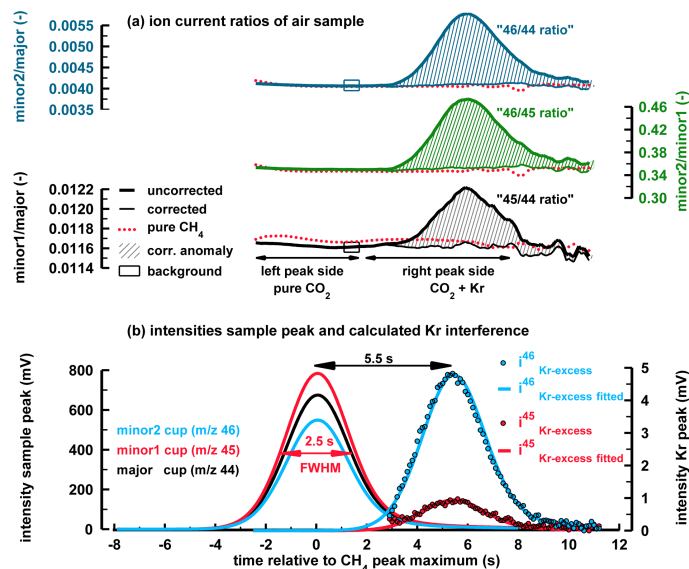


**Fig. 11.** Compilation showing the principle of the Kr correction for an air sample measured with the AWI-system. **(a)** Ion current ratios in bold lines are the uncorrected ratios, the rectangle indicates the time interval that is used to determine the background to calculate the Kr interference shown in the panel below. The thin line and the hatched area show the ratio after the Kr correction, i.e. after the subtraction of the fitted Kr peak from the measured ion current. The red dotted line is the ratio of pure  $\text{CH}_4$  without Kr interference. The “46/45 ratio” serves as an independent visual check whether the correction was successful since the anomaly of this ratio is not used for the correction method. **(b)** Intensities for the three Faraday cups of the  $\text{CH}_4$  sample (left axis). The interference calculated from the anomalies plotted in the ratios above (right axis) with the dots representing the calculated raw anomaly for  $m/z$  45 and  $m/z$  46, the lines are a fit to the respective data used for correction.

## Kr interference during carbon isotope analysis

J. Schmitt et al.

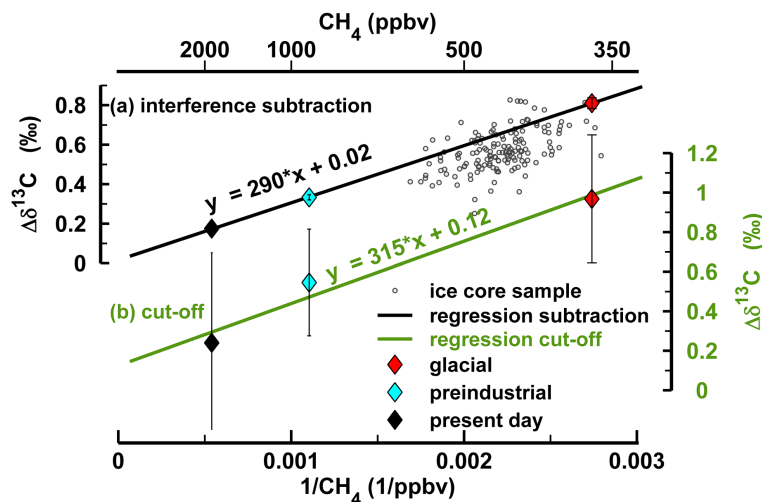


**Fig. 12.** Comparison of two methods to account for the Kr interference based on measurements with the AWI system using the three intercomparison cylinders with contrasting  $\text{CH}_4/\text{Kr}$  mixing ratios. Plotted are the  $\Delta\delta^{13}\text{C}$  numbers, i.e. the differences between the original results and the results obtained after removing the Kr effect. Both methods reveal that with decreasing  $\text{CH}_4$  concentrations (hence,  $\text{CH}_4/\text{Kr}$  mixing ratios)  $\Delta\delta^{13}\text{C}$  becomes larger. **(a)** Results for the method of Sect. 5.4, where the Kr interference is subtracted from the raw data time series. Coloured diamonds with error bars mark the cylinder measurements, grey circles show a data set of 152 ice core measurements. **(b)** Results for the relatively simple method, where the right integration boundary is shifted from 10 s to 3 s after the  $\text{CH}_4$  peak maximum to cut-off a large fraction of the Kr peak. This method is more vulnerable to peak shape variations leading to more noise to the results.

Title Page

Abstract

Introduction

Conclusions

References

Tables

Figures

◀

▶

◀

▶

Back

Close

Full Screen / Esc

Printer-friendly Version

Interactive Discussion



## Kr interference during carbon isotope analysis

J. Schmitt et al.

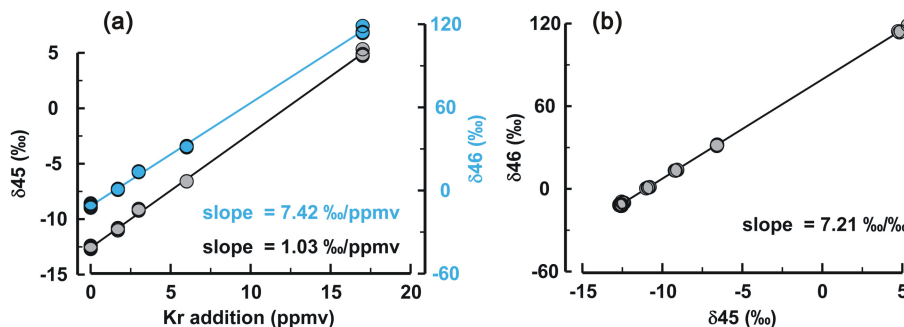


**Fig. 13.** Results of artificially adding pure Kr to a  $\text{CH}_4$  sample. **(a)** Both isotope ratios show a linear relation of the  $\delta$  values with the amount of Kr added. **(b)** The isotope ratios are closely correlated ( $r^2 = 1.00$ ) and this relation can be used to correct for the Kr interference without knowing the exact  $\text{CH}_4$ -Kr mixing ratio of a sample. Note that here the  $\delta_{46}/\delta_{45}$  slope is shown, i.e. the inverse value used in Eq. (9).

Title Page

Abstract

Introduction

Conclusions

References

Tables

Figures

◀

▶

◀

▶

Back

Close

Full Screen / Esc

Printer-friendly Version

Interactive Discussion

